European Journal of Medicinal Chemistry 246 (2023) 114942

Contents lists available at ScienceDirect

European Journal of Medicinal Chemistry

journal homepage: www.elsevier.com/locate/ejmech

Research paper

Rational design of novel nucleoside analogues reveals potent antiviral agents for EV71

Martina Salerno [a], Carmine Varricchio [b], Federica Bevilacqua [b], Dirk Jochmans [c], Johan Neyts [c], Andrea Brancale [b], Salvatore Ferla [d], Marcella Bassetto [a,*]

[a] Department of Chemistry, College of Science and Engineering, Swansea University, Swansea, SA2 8PP, UK
[b] School of Pharmacy and Pharmaceutical Sciences, Cardiff University, Cardiff, CF10 3NB, UK
[c] KU Leuven – Rega Institute, Department of Microbiology, Immunology and Transplantation, Leuven, Belgium
[d] Medical School, Faculty of Medicine, Health and Life Science, Swansea University, Swansea, SA2 8PP, UK

ARTICLE INFO

Keywords:
Novel small-molecule antiviral agents
METTL3
EV71
Molecular modelling
Synthetic organic chemistry
Prodrugs

ABSTRACT

Different viruses belonging to distinct viral families, such as enterovirus 71, rely on the host methyltransferase METTL3 for the completion of fundamental cytoplasmic stages of their life cycle. Modulation of the activity of this enzyme could therefore provide a broad-spectrum approach to interfere with viral infections caused by viruses that depend on its activity for the completion of their viral cycle. With the aim to identify antiviral therapeutics with this effect, a series of new nucleoside analogues was rationally designed to act as inhibitors of human METTL3, as a novel approach to interfere with a range of viral infections. Guided by molecular docking studies on the SAM binding pocket of the enzyme, 24 compounds were prepared following multiple-step synthetic protocols, and evaluated for their ability to interfere with the replication of different viruses in cell-based systems, and to directly inhibit the activity of METTL3. While different molecules displayed moderate inhibition of the human methyltransferase *in vitro*, multiple novel, potent and selective inhibitors of enterovirus 71 were identified.

1. Introduction

Enterovirus 71 (EV71) is a non-enveloped, single stranded positive sense RNA virus belonging to the *Picornaviridae* family [1]. The RNA genome encodes for a large polyprotein, cleaved in three precursors, which are then further hydrolysed resulting in four structural and seven non-structural proteins [2]. EV71 is the main cause of the hand foot and mouth disease (HFMD), which is commonly spread in children under the age of five [3]. Individuals are infected through the alimentary tract, and the infection can be transmitted by coming into contact with secretions of an infected individual [4]. Infection can range from being asymptomatic, to HFMD, to severe neurological symptoms, with high mortality rates in severe cases [5]. The development of severe neurological symptoms appears related to the release of small extracellular vesicles containing EV71 components during the early stages of the infection. *In vitro* studies have confirmed that these vesicles can cross the blood-brain barrier, causing the infection to spread to the central nervous system [6]. EV71 infections have become a major public health problem in China, where 15 million possible cases of HFMD were reported between 2013 and 2019 [7]. In this country, three prophylactic vaccines are currently exclusively licensed and marketed [8], but an established treatment for EV71 infections is still unavailable. Different antiviral agents have been explored [9,10], mainly targeting the viral 3C protease [11], but no candidate antiviral drugs are currently at any stages of clinical development [12].

Nucleotide and nucleoside analogues have been widely investigated as antivirals for EV71 infections, as they exhibit potent antiviral activities against several viruses [13,14]. In the context of EV71 antiviral research, N^6-benzyladenosine (BAPR) **1**, whose structure is shown in Fig. 1, has been previously found to selectively inhibit EV71 replication in cell-based assays [15]. In a follow-up study, the antiviral activity of this compound was improved by substitution with a trifluoromethyl group in the *meta* position of the benzyl ring (compound **2** in Fig. 1), which significantly enhanced both the antiviral effect and the selectivity index of this scaffold, whose antiviral mechanism of action has not been elucidated yet [16]. The adenosine nucleoside analogue **NITD008**, a selective inhibitor of replication of *Flaviviruses* [17], has also been found to effectively inhibit EV71 replication in cell-based assays, acting as a

* Corresponding author.
E-mail address: marcella.bassetto@swansea.ac.uk (M. Bassetto).

https://doi.org/10.1016/j.ejmech.2022.114942
Received 15 September 2022; Received in revised form 23 October 2022; Accepted 16 November 2022
Available online 24 November 2022

chain terminator on the viral RdRp [17]. Finally, the phosphoramidate prodrug remdesivir has recently been shown to inhibit EV71 replication [18].

Adenosine methylation at its N^6 position (m6A), to form N^6-methyladenosine, is one of the most abundant RNA modifications [19,20]. During viral replication, this modification at specific positions of the viral genome constitutes a key factor for viral RNA translation, by recruitment of host factors, or for promoting infection by protecting the viral RNA from immune system detection [21]. As EV71 does not encode for a methyltransferase on its own, the m^6A modification needs to be carried out by host factors, as it is fundamental for the success of viral replication. The METTL3/METTL14 methyl transferase complex has recently been demonstrated as the host factor responsible for the m^6A modification of the EV71 viral genome [22], according to a mechanism that includes direct interaction with the viral RNA-dependent RNA polymerase (RdRp) in the cytoplasm [23]. Furthermore, knockdown of METTL3 results in reduced EV71 replication in cell-based assays [22]. Additionally, the METTL3/METTL14 complex has recently been demonstrated as essential for the replication of hepatitis C virus (HCV) and hepatis B virus (HBV) [24], and as an antiviral target to control herpes simplex virus type 1 (HSV-1) infections [25]. This evidence suggests the potential exploitation of host METTL3 as a broad-spectrum target to interfere with the replication of those viruses with cytoplasmic replication cycles, including SARS-CoV-2. Indeed, it has recently been reported that METTL3 carries out adenosine N^6-methylation (m6A) modifications of SARS-CoV-2 RNA, which are responsible for a reduced sensing and consequent activation of the immune system, confirming the suitability of METTL3 to interfere with the early stages of SARS-CoV-2 infections [26].

The METTL3/METTL14 complex regulates aspects of the cell cycle such as RNA metabolism, translation and processing [27,28], and it has previously been proposed as a druggable target for its role in cancer development: the complex acts as an oncogene, promoting the growth and progression of both hematopoietic and solid cancers (including acute myeloid leukaemia, liver, gastric and lung cancer) [29]. In two recent studies, the first inhibitors of this complex have been reported (Fig. 2). In particular, different adenosine analogues have been proposed as potential inhibitors of METTL3, with the most potent of them, compound **3**, exhibiting an IC_{50} of 8.7 μM [30]. In 2021, the structure of **4** was reported as a non-SAM-like potent inhibitor of METTL3, with an IC_{50} of 16.9 nM, to be potentially used in the treatment of myeloid leukaemia [31]. Compound **4**, which was identified with a high-throughput screening, has been tested *in vivo*, showing no toxicity associated to its administration, suggesting the inhibition of METTL3 as a safe therapeutic approach in drug discovery.

Targeting a host factor such as the METTL3/METTL14 complex to develop antiviral agents might result in greater risk of toxicity and side effects, as its inhibition would possibly interfere with normal cell metabolism. This is a common potential disadvantage of host-directed antiviral strategies [32], and the complex has indeed been described to have an important role in sustaining immune natural killer cell numbers and maturation [33]. However, as the potent METTL3 inhibitor **4** has not shown any toxic side effects or weight loss in mice when tested *in vivo* [31], safety data available so far appear to confirm inhibition of this complex represents a safe strategy to discover new drugs. Targeting a host factor, such as this complex, for the development of antivirals can offer the advantage to prevent the insurgence of drug resistance, and can potentially support the development of broad-spectrum agents [34]. Although its role in the replication of different viruses has been recently confirmed [22–25], to the best of our knowledge, no inhibitors of the METTL3 enzyme have yet been evaluated as potential antiviral agents.

This work aimed to rationally design and synthesise new nucleoside analogues with the potential to bind the SAM pocket of human METTL3 enzymes and inhibit their function, as a novel, host-directed strategy for viral infections caused by viruses that rely on its activity for completing essential stages of their life cycle, such as EV71. Such compounds would validate the inhibition of METTL3/METTL14 as a new, potentially broad-spectrum antiviral strategy, and they could provide the starting point to develop novel therapeutics to treat a range of viral infections. Following this approach, the structures of known non-selective, SAM-dependent methyltransferase inhibitors were rationally modified to incorporate structural features that could confer selectivity for METTL3, in addition to cell permeability. This led to the design of novel nucleoside analogues with an optimal predicted ability, according to molecular docking studies, to bind the SAM/SAH site of human METTL3. Optimised multiple-step synthetic routes enabled the synthesis of all the designed molecules, which were subsequently evaluated for their ability to interfere with the replication of different viruses in cell-based assays, and for the direct inhibition of METTL3 enzymatic activity. Most of the compounds evaluated interfere at least in part with the enzyme activity at relatively high micromolar concentrations, with three novel analogues displaying IC_{50} values in the micromolar range. Different new

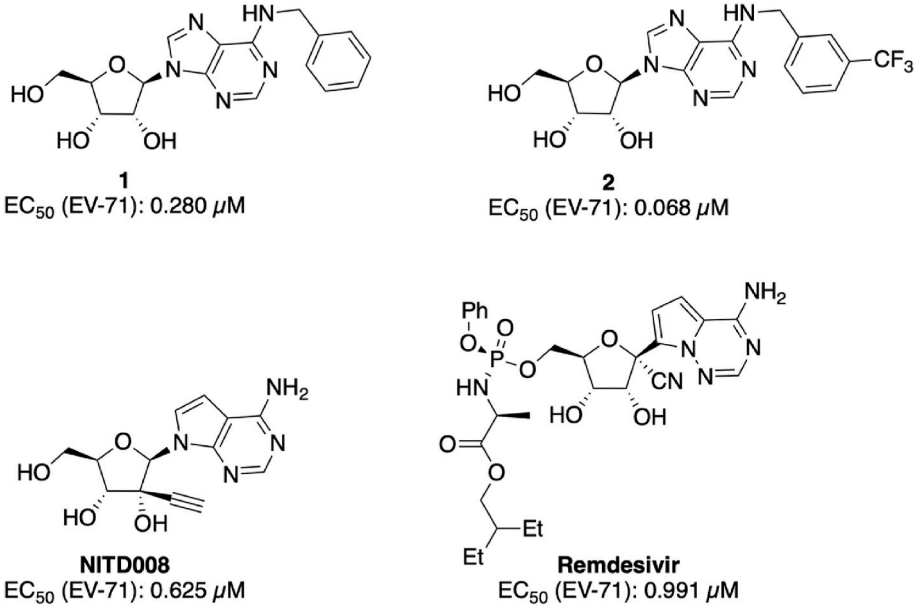

Fig. 1. Chemical structures of previously reported nucleoside analogues active as inhibitors of EV71 replication.

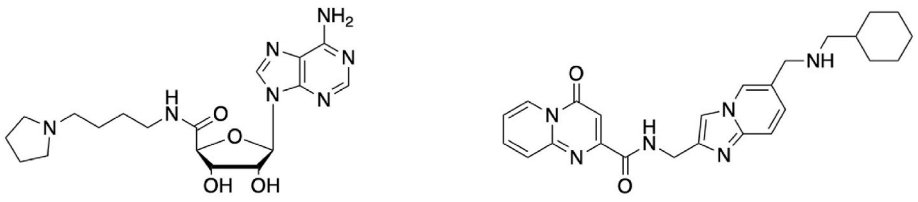

3
IC_{50} (METTL3): 8.7 μM

4
IC_{50} (METTL3): 16.9 nM

Fig. 2. Chemical structure of previously reported inhibitors of the METTL3 methyl transferase.

molecules were found to selectively inhibit the replication of EV71 in cell-based systems, with EC_{50} values in the sub-micromolar range, while a subsequent series of phosphoramidate prodrugs of selected antiviral nucleoside analogues revealed a nanomolar inhibitor of EV71 replication in cell-based assays.

2. Results and discussion

2.1. Rational design of potential selective inhibitors of human METTL3 and molecular docking studies

The METTL3/METTL14 complex is an asymmetric heterodimer (Fig. 3a), in which METTL3 is the catalytic subunit, while METTL14 supports RNA-binding [35]. The two subunits interact by an extensive groove of hydrogen bonds, which, being rich in positively charged residues, is thought to accommodate the RNA [36].

The crystal structure of human METTL3/METTL14 in complex with SAM (PDB ID 5IL1) was inspected to analyse the binding interactions with the substrate, and to evaluate the potential presence of specific structural features that could guide the design of selective inhibitors. METTL3 binds SAM in a site facing a conserved Asp-Pro-Pro-Trp motif, required for MTase activity [37], as shown in Fig. 3b. In addition, SAM interacts with other fundamental amino acids present in the catalytic domain of METTL3. In particular, the adenine moiety interacts via a

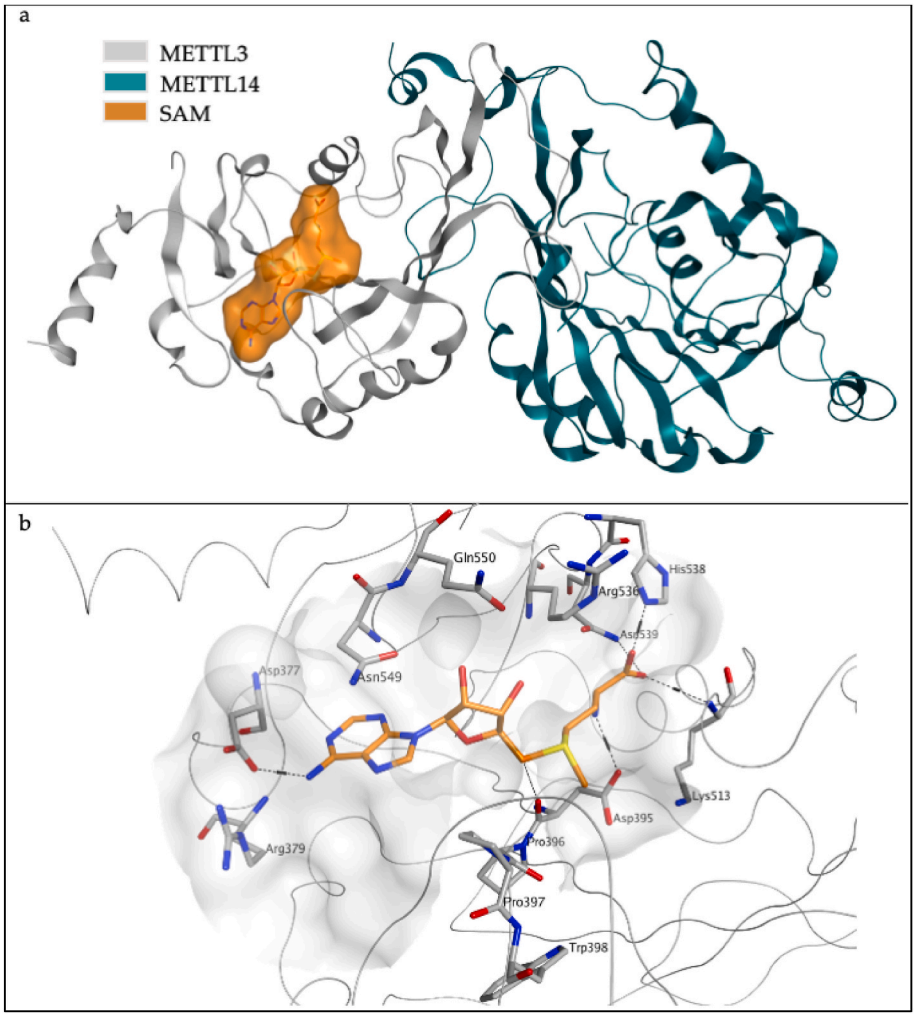

Fig. 3. Crystal structure of METTL3/METTL14 in complex with SAM (PDB ID 5IL1). a) Ribbon representation of the complex with the SAM substrate highlighted as orange molecular surface. b) SAM binding site area in the METTL3 subunit, represented as grey molecular surface. The SAM substrate is represented with carbon atom in orange, while METLL3 is represented as a thin grey ribbon and carbon atoms in grey.

hydrogen bond with the side chain of Asp377, while the hydroxyl groups of the ribose sugar make hydrogen-bond contacts with Asn549, Gln550 and Arg536. Asp395, His538, Asn539 and Lys513 interact directly with the methionine moiety of SAM (Fig. 3b) [36].

Interestingly, the SAM binding pocket presents an extension of its unoccupied surface at the level of the adenine nucleobase, as highlighted in Fig. 4. This additional sub-pocked is centred around the sidechain of Arg379.

Interestingly, the presence of a similar hydrophobic pocket next to the SAM binding site of *Flavivirus* MTases has previously enabled the identification of a SAH-based inhibitor of dengue virus (DENV) methyltransferase, compound **5** in Fig. 4, with a high level of selectivity over human MTases [38]. Similarly to the known anti-EV71 compounds **1** and **2**, the dengue MTase inhibitor **5** is characterised by the presence of a benzyl-substituent at position N^6 of the adenine nucleobase. Therefore, due to the presence of Arg379 at the surface of the METTL3 additional sub-pocket, the design of nucleoside analogues with a benzyl-substitution at the N^6 position of the nucleobase was envisaged, to fill this portion of the space, while potentially enabling an additional cation–π interaction between Arg379 and the novel molecules.

Following these observations, the structures of known SAM-dependent, pan-MTase inhibitors methylthioadenosine (MTA) [39] and *S*-tubercidinyl-L-homocysteine (TubHcy) [40], which is the 7-deaza analogue of S-adenosylhomocysteine (SAH), were chosen as a starting point for rational modification of their scaffold, with the insertion of a functionalised benzyl-substituent at the N^6 position (Fig. 5). As a significant limitation to the evaluation of compounds such as **5** and TubHcy in cell-based antiviral assays is their lack of cell permeability, an important feature in the design of novel potential METTL3 inhibitors was the presence of a cell-permeable scaffold, which would enhance a potential antiviral effect in cell systems, as summarised in Fig. 5. In particular, to confer permeability to the structures of the novel compounds designed, a methyl-thio substitution at the 5' position of the ribofuranose ring was envisaged (compounds **6**–**8**), or alternatively a double-protected homocysteine group at this position (**9**), with a methyl ester group masking the free carboxylic acid, and a trifluoroacetamide group masking the free amine function, as these combined modifications had been identified in the past as a successful strategy for enhancing the cell permeability of TubHcy [40].

The newly designed compounds are predicted to achieve an optimal occupation of the SAM binding pocket of METTL3, as confirmed by molecular docking studies performed for **6**–**8**, and the deprotected homocysteine analogue of **9**, on the substrate site of the 5IL1 crystal structure, using the Glide SP docking program [41] (Fig. 6). The additional benzyl group of the newly designed compounds sits in close proximity to Arg379, at a distance range that can support a direct cation–π interaction. From this analysis, the presence of a *meta*-substituent in the benzyl ring appears to be correlated with the best predicted occupation of the additional sub-pocket, as revealed by the docking poses found for compounds **6a-c**, **7a** and the deprotected form of **9**. When the chloro-substituent is moved from the *meta* (**6a**) to the *ortho* position in **6e**, although the benzyl group achieves good proximity to Arg379, an overall perturbation of the predicted binding is observed, with the loss of most of the contacts found for the other compounds in the series. Positioning of this substituent to the *para* position of the benzyl ring appears to be associated with a similar effect of perturbation of the overall binding of the scaffold. An analogous detrimental effect on binding overall appears to be associated with the insertion of an extra methyl group at the benzylic position in compounds **6g-h**, with a more pronounced negative impact on predicted binding found for **6h**, where the additional modification is combined with a chloro-substituent at the *ortho* position of the benzyl ring. Finally, the new modification designed in compound **8** also appears to be the detrimental for the overall occupation of the binding area, with the fused indoline ring only partially occupying the additional sub-pocket, remaining at a higher distance from the sidechain of Arg379 in comparison with all the other analogues designed, and with the loss of most contacts found for the other compounds. All the newly designed molecules were still selected for chemical synthesis and antiviral evaluation, including those associated with a negative effect on predicted binding to METTL3, as they were envisaged as a potential negative control to confirm the reliability of the docking predictions.

2.2. Synthesis of the newly designed compounds

The newly designed nucleoside analogues were synthesized according to two-to six-step synthetic routes. The synthesis of target compounds **6**–**8** is summarised in Scheme 1. Briefly, for the preparation of **6a-h**, two alternative strategies were followed. Both approaches started with the conversion of 6-chloro-9-(β-D-ribofuranosyl)purine **10** into the N^6-benzyl adenosine analogues **2**, **11a-b** and **11d-h**, by reacting **10** with an excess of the appropriate, differently substituted benzylamine in EtOH, while heating in a sealed tube, modifying a previously reported method [42]. Target products **6a-c** were prepared by directly treating the respective ribosides **11a-b** and **2** with methyl disulphide and tributylphosphine in anhydrous DMF at room temperature, according to a

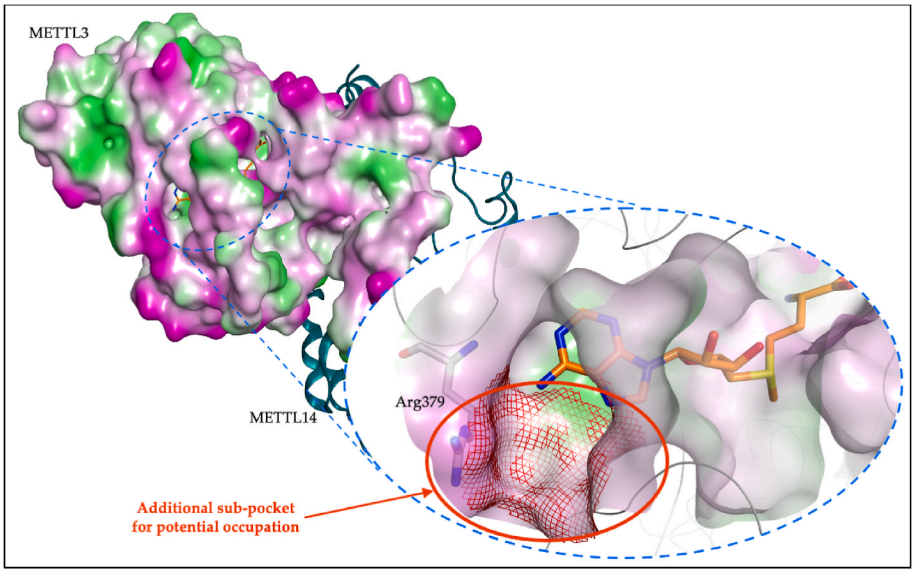

Fig. 4. Zoom on the SAM binding area in the 5IL1 crystal structure, with highlighted an additional sub-pocket at the level of the adenine nucleobase, centred around Arg379. METTL14 is represented as thick green ribbon. METTL3 is represented as lipophilic/hydrophilic molecular surface (pink = hydrophilic, green = lipophilic, white = neutral), thin grey ribbon and carbon atoms in grey (Arg379). The SAM ligand is represented with carbon atoms in orange. The surface of the additional sub-pocket is rendered in a red-line representation.

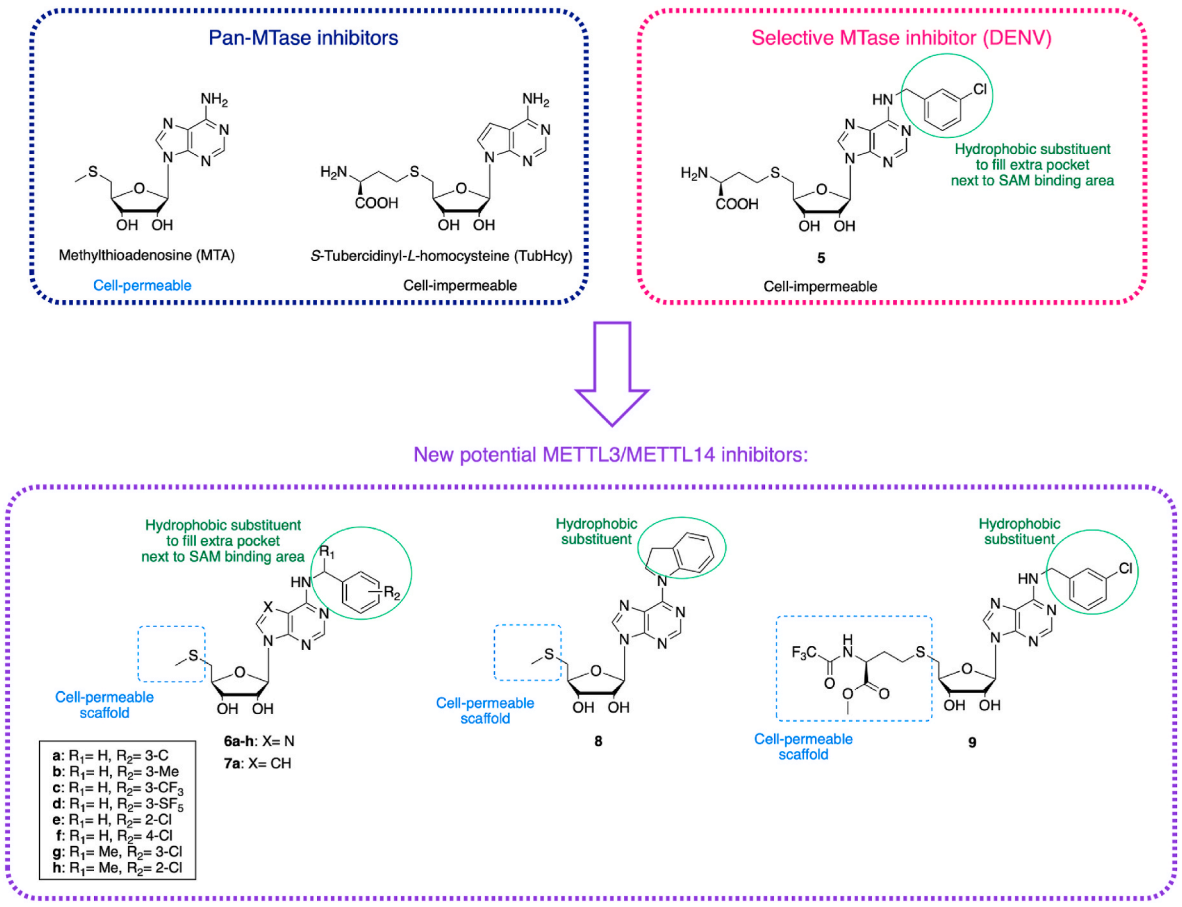

Fig. 5. Chemical structures of known pan-MTase inhibitors of SAM-dependent MTases, of the SAH analogue that selectively targets DENV MTases thanks to its additional hydrophobic substituent (**5**), and of the novel target compounds designed in this study to target human METTL3 enzymes (**6**–**9**). The structural features considered for the design of the novel compounds are highlighted: a cell-permeable structural feature at the level of the ribofuranose part of the scaffold, and a functionalised N^6-benzyl substituent, to occupy the additional space next to the SAM binding area in the structure of METTL3.

literature procedure [43]. This direct strategy was associated with moderate yields and relative complex chromatographic purifications required for the final products, therefore an alternative pathway was followed for compounds **6d-h**: the corresponding ribosides **11d-h** were converted into the 5′-chlorides by reaction with thionyl chloride in MeCN, in the presence of pyridine as a base [42]. Finally, following a reported procedure [44], the chlorides were treated with sodium thiomethoxide in anhydrous DMF, to afford the desired final products **6d-h**.

Preparation of the novel 7-deazapurine analogue **7a** started with the synthesis of tubercidin **15**, from 1-*O*-acetyl-2,3,5-tri-*O*-benzoyl-β-D-ribofuranose **13**, which was coupled with 6-chloro-7-deazapurine according to a Vorbrüggen glycosylation [45], which starts with the silylation of the nucleobase using *N*,*O*-bis(trimethylsilyl)acetamide (BSA) in acetonitrile, followed by the addition of the sugar **13** and catalyst TMSOTf, which activates the ribofuranose, yielding the benzoyl-protected nucleoside **14**. Simultaneous deprotection of the benzoyl groups and displacement of the chloride leaving group at position 6 of the nucleobase was achieved by treating **14** with ammonium hydroxide while heating in 1,4-dioxane in a sealed tube, to afford **15** in good yield. The two-step conversion of tubercidin **15** into the corresponding N^4-3-chlorobenzyl derivative **17** was achieved according to a previously reported protocol [46], by which **15** was treated with 3-chlorobenzylbromide in anhydrous DMF while heating, to obtain the structural isomer **16** first, which was then converted into the desired intermediate **17** by addition of a THF solution of dimethylamine and refluxing the mixture in methanol. A first attempt to directly convert **17** into **7a** by reaction with methyl disulphide in the presence of tributylphosphine failed, therefore **17** was converted into the corresponding 5′-chloride **18** with thionyl chloride in the presence of pyridine, followed by treatment of **18** with sodium thiomethoxide in anhydrous DMF at room temperature. Preparation of indoline analogue **8** followed the same three-step approach applied for final products **6d-h**, with the only difference that indoline replaced the substituted benzylamines used in the first synthetic step for the functionalisation of **10** at position 6.

The synthetic preparation of cell-permeable SAH-analogue **9** is described in Scheme 2.

The route to obtain **9** began with the conversion of both carboxylic acid groups of L-homocystine **21** to the corresponding methyl ester **22**, which was performed using thionyl chloride in MeOH as previously reported [42]. Next, the two free amine groups were converted to trifluoroacetamide in **23**, by treating **22** with trifluoroacetic anhydride while heating the mixture to 60 °C [42]. Finally, the N^6-functionalised riboside **11a** was directly reacted with **23** in the presence of tributylphosphine in anhydrous DMF, to afford the target product **9** in modest yield after chromatographic purification.

2.3. Biological assays

2.3.1. Antiviral and cytotoxicity studies

The new target molecules **6**–**9** were evaluated against the replication of a small panel of viruses in cell-based assays, which also enabled the evaluation of the compounds' cytotoxicity. Due to the reported anti-EV71 effect of **2** [16], synthetic intermediates **11a-b**, **11d-h**, **17** and **19** were also evaluated in these assays, along with compound **2**, which was used as a positive control for the antiviral effect on EV71. Rupintrivir was also included as positive control for the EV71 assay [47]. The

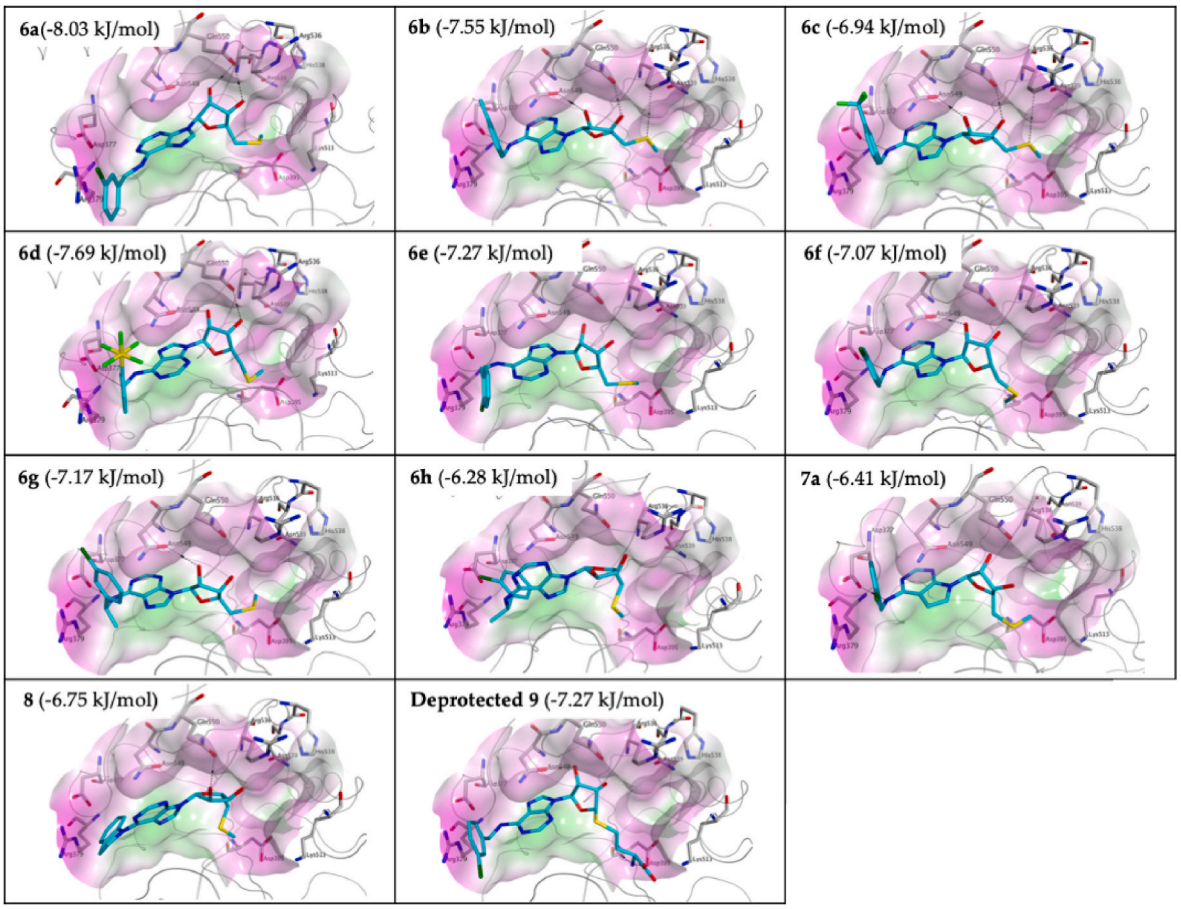

Fig. 6. Predicted binding of the novel analogues to the SAM binding pocket of the METTL3/METTL14 complex crystal structure 5IL1, evaluated with the molecular docking program Glide SP [41]. Most newly designed compounds show the potential to achieve an optimal fitting of the substrate binding site, with the possibility of forming direct cation–π contacts with Arg379. Additional residues that may stabilise the binding of this portion of the new compounds are Asp377, Asn549, Gln550, Arg536, Asp395, His538, Asn539 and Lys513. METTL3 is represented as lipophilic/hydrophilic molecular surface (pink = hydrophilic, green = lipophilic, white = neutral), thin grey ribbon and carbon atoms in grey. The newly designed potential ligands are represented with carbon atoms in light blue. Glide SP docking scores are specified in brackets.

test compounds were evaluated in a EV71-induced cytopathic effect (CPE) reduction assay, in rhabdomyosarcoma (RD) cells, as previously reported [16]. Then, due to the role of the METTL3/METLL14 complex recently demonstrated for the life cycle of SARS-CoV-2 [26], the compounds were also evaluated in a cell viability assay using a fully replication-competent SARS-CoV-2 ancestral Wuhan strain in Vero E6 cell culture, where variations in the cytopathic effect caused by SARS-CoV-2 are assessed in the presence and in the absence of the test compounds, while also monitoring changes in cell viability induced by the potential cytopathic effect of the test compounds on their own [48]. Remdesivir was used as positive control for the evaluation of antiviral activity against SARS-CoV-2. Finally, as the novel molecules prepared have the potential to fit the SAM binding pocket of *Flavivirus* MTases similarly to **5** (as detailed in Fig. S1 and Fig. S2 of the Supporting *Information*), the test compounds were also evaluated against the replication of Zika virus as a model *Flavivirus*. For this evaluation, a ZIKV-induced CPE-reduction assay was performed using Vero E6 cells, using 7-deaza-2′-C-methyladenosine (7-DMA) as a positive control [49]. For these assays, toxicity of all the test compounds was evaluated in parallel, on treated-uninfected cells. The results obtained from this screening are shown in Table 1.

All the compounds tested showed selectivity for EV71, as none of them interfered with the replication of SARS-CoV-2 or Zika virus, even at relatively high concentrations of 100 μM. Most of the compounds evaluated showed instead a clear antiviral effect against EV71, with EC_{50} values ranging from the high nanomolar to the low micromolar range. Most of the novel nucleoside analogues featuring a thiomethyl group at the 5′-position of the ribose sugar (compounds **6**–**8**) displayed an antiviral effect against EV71 in the low micromolar or submicromolar range, with compounds **6c**, **6h** and **7a** representing an exception to this trend, as they were found completely inactive. The lack of activity found for **6h** appears to be in line with the molecular docking predictions, as the modification at the benzylic portion of the molecule was associated with an overall perturbation of predicted binding to METTL3. Of the remaining analogues with the 5′-thiomethyl scaffold, **8** is the least potent in the series, with an EC_{50} value in the range of 20 μM. Also this result appears to be in line with our molecular docking predictions. The best analogue found in this group of molecules is **6a**, with a *meta*-chloro substituent at the benzyl ring, which shows a submicromolar EC_{50} against EV71, followed by **3b**, with a 3-methyl substituent group at this position, and by **6d**, where the substituent on the benzyl is a *meta*-pentafluorosullfanyl group. **6d** however is associated with an increased cytotoxic effect compared to the other analogues in the series, which can also be observed in the Vero E6 cell line. This toxicity appears to be associated with the concomitant presence of a pentafluorosulfanyl substituent at the benzyl ring, and a 5′-thiomethyl substituent in the ribose part of the molecule, as the corresponding 5′-OH analogue, **11d**, does not show any cytotoxic effect at the test concentrations in both cell lines. The loss of activity found for **6e** and **6f** compared to **6a** seems to suggest that the *meta*-position is ideal for the benzyl-ring substituent, while a range of substituents appear to be tolerated at this position, as indicated by the results obtained for **6b** and

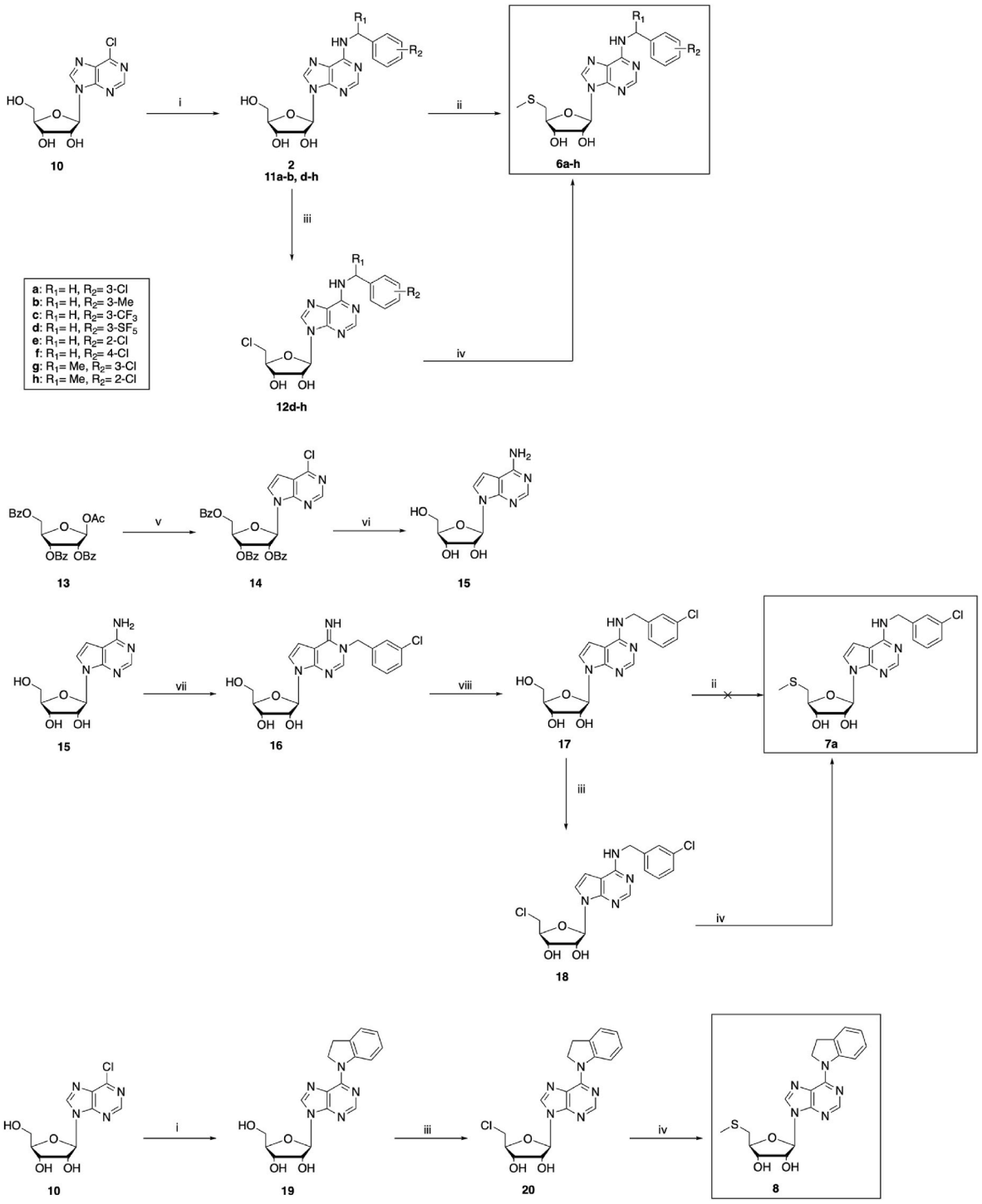

Scheme 1. Preparation of target compounds **6**–**8**. *Reagents and conditions*: (i) substituted benzylamine, EtOH, 70 °C, sealed tube, 24 h (82–96%); (ii) $(MeS)_2$, P(*n*-Bu)$_3$, DMF, r.t., 48 h (40–57%); (iii) $SOCl_2$, Pyr, MeCN, 0 °C (4 h) to r.t., o.n. (50–76%); (iv) MeSNa, DMF, r.t., o.n. (43–81%); (v) 6-chloro-7-deazapurine, BSA, TMSOTf, MeCN, r.t. to 50 °C, o.n. (45%); (vi) NH_4OH, 1,4-dioxane, 110 °C, sealed tube, 4 h (65%); (vii) 3-chlorobenzylbromide, DMF, 75 °C, 24 h; (viii) Me_2NH, THF, MeOH, reflux, o.n. (75% over two steps).

6d, although compound **6c** represents a clear exception to this trend. Replacement of adenine N^7 with a carbon to mimic the structure of tubercidin in **7a** is associated to a complete loss of anti-EV71 effect in the 5′-thiomethyl series of structures, but this trend is not confirmed for the 5′-OH analogues. The novel, cell-permeable L-homocysteine analogue **9** also showed a selective anti-EV71 profile without displaying significant cytotoxicity, with an EC_{50} value in the low micromolar range.

Although good anti-EV71 profiles can be confirmed for different of the newly designed compounds **6**–**9**, the most potent analogues found in this group of molecules are the 5′-OH synthetic intermediates **2**, whose anti-EV71 activity was already known [16], **11** and **17**. With the exception of **11h** and **19**, whose complete lack of antiviral activity is in line with the results obtained for their 5′-thiomethyl counterparts and with the molecular docking predictions, all the 5′-OH analogues tested displayed a significantly improved activity compared to the corresponding 5′thiomethyl produtcs, with most of them displaying EC_{50}

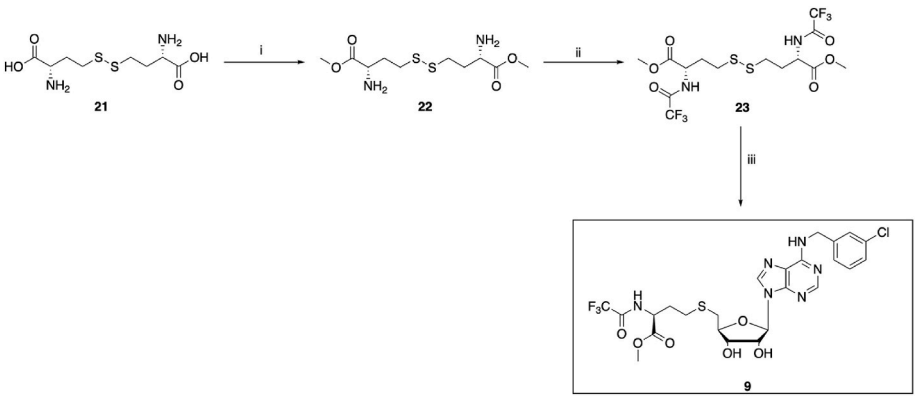

Scheme 2. Preparation of target compound **9**. *Reagents and conditions*: (i) $SOCl_2$, MeOH, 0 °C–80 °C, 3 h; (ii) $(CF_3CO)_2O$, 60 °C, 3 h (94% over two steps); (iii) **11a**, P(*n*-Bu)$_3$, DMF, r.t., 48 h (21%).

values in the sub-micromolar or high nanomolar range. Although **2** remains the most potent compound in this series, also associated with a complete lack of toxicity at the test concentrations, different other analogues displayed a similarly potent anti-EV71 effect, with the best profiles found for **11b** and **17**. The trend in activity variations associated with structural modifications does not match the one previously observed for the 5′-thiomethyl analogues. Replacement of the adenine N^7 with a carbon in **17** appears to lead to an improvement in antiviral activity compared to **11a**, and movement of the chloro-substituent from the *meta* (**11a**) to the *ortho* position (**11e**) appears to be tolerated, although placing the substituent at the *para* position is still associated with a reduced activity (**11f** versus **11a**). However, **11e** appears to display some cytotoxicity in the RD cell line. The insertion of an extra methyl group at the benzylic position of **11a**, in compound **11g**, seems to be associated with a reduced antiviral activity, with a similar effect for both the 5′-OH (**11g** versus **11a**) and the 5′-thiomethyl (**6g** versus **6a**) series of compounds. In addition to **11e**, the only other analogue in this group of molecules that shows some cytotoxic effect in the RD cell line is **11a**, with a CC_{50} in the range of 40 μM, but its selectivity index remains high (>400).

2.3.2. METTL3/METTL14 enzymatic assay

In order to investigate whether the anti-EV71 effect observed for the molecules prepared in this study is indeed associated to an interference with the enzymatic activity of METTL3, a selection of eight compounds was tested *in vitro* using the HotSpot℠ platform for methyltransferases available at Reaction Biology Corporation [51]. For this analysis, **6a**, **6d**, **6e**, **11a**, **11b**, **11c**, **11d** and **17** were incubated with the METTL3/-METTL14 complex and a ssRNA substrate for 30 min before addition of tritium-labelled *S*-adenosyl-methionine functioning as labelled-methyl donor. Activity was evaluated by detection of methylated-labelled ssRNA by a filter binding method and reported as percentage of methyltransferase activity. The eight compounds were tested at an initial concentration of 100 μM, showing the activity reported in Table 2. *S*-Adenosyl homocysteine (SAH) was used as positive control [52].

All the compounds tested demonstrated partial inhibition of the complex at this concentration. For the two showing the highest percentage inhibition at 100 μM, **6a** and **17**, dose-response curves were obtained, from which it was possible to calculate IC_{50} values, as reported in Fig. 7. The dose response curve obtained for SAH is reported in the Supporting *Information* (Fig. S3).

Despite the test compounds clearly show the potential to inhibit the activity of the METTL3/METLL14 complex, with the most potent analogue found (**17**) showing an inhibitory IC_{50} in the micromolar range, the high IC_{50} values identified for **6a** and **17** compared to their anti-EV71 EC_{50} values, which are in the sub-micromolar and nanomolar range respectively, appear to indicate that the main antiviral mechanism of these molecules is likely a different one, rather than the direct inhibition of METTL3 enzymatic activity, possibly the direct inhibition of a viral protein. In addition, this hypothesis appears to be further confirmed by the marked selectivity observed for EV71 in the antiviral assay, which may indeed be due to direct interference with a viral target as main mechanism of action. As the molecules are all nucleoside analogues, a likely direct viral target is represented by the viral polymerase, and this is in line with the higher activity observed for the 5′-OH analogues compared to the 5′-SMe analogues in the antiviral experiments. If the compounds do inhibit the viral polymerase of EV71, their active form is likely to be the nucleoside triphosphate.

2.4. Further synthetic chemistry and biological evaluations

The potent, selective antiviral effect observed for intermediate **17** against the replication of EV71 prompted us to design a novel modified tubercidin analogue, which features the presence of the same 3-trifluoromethylbenzyl substituent at position N^6 present in **2** (compound **25** in Scheme 3). In addition, due to the potent, superior antiviral activity found for different riboside intermediates compared to their 5′-methylthio counterparts (e.g. **2** versus **6c**), our hypothesis is that, at least the 5′-OH analogues, may likely have a direct antiviral effect, possibly inhibiting the viral polymerase, as happens for most nucleoside analogues that act as direct-acting antivirals [13,14]. As the compounds would likely require metabolic activation to their triphosphate form to inhibit the viral polymerase, as a means to obtain an indirect confirmation of their inhibition of this target, we planned to modify the structure of our active compounds to insert a chemical feature that would facilitate the formation of the triphosphate analogues in cells. A small series of novel phosphoramidate prodrugs was therefore planned (compounds **27**–**28** in Scheme 3), considering in a first instance the parent ribosides **2** and **25**, as a means to potentially boost their antiviral effect, and indirectly obtain a confirmation that the active form is the 5′-triphosphate analogue, and that they may therefore target the viral polymerase as their main mechanism of action [53].

Target riboside **25** was obtained according to the same route followed for **17**, using 3-trifluoromethylbenzylbromide in the first stage of the reaction. Novel phosphoramidate prodrugs **27**–**28** were obtained following a coupling reaction between the appropriate nucleoside analogues **2** and **25** and the aryl amino acid phosphorochloridate **26**, in the presence of *N*-methylimidazole (NMI), according to a previously established procedure [54]. **26** was prepared from the corresponding benzyl ester of L-alanine, which was reacted with phenyl dichlorophosphate, as previously described [54].

The three additional compounds were evaluated for their antiviral properties against EV71 and SARS-CoV-2 in cell-based systems, while **25** was also evaluated for its potential inhibition of Zika virus replication in cells. The results obtained are summarised in Table 3.

The novel tubercidin analogue **25** displayed a sub-micromolar,

Table 1
Antiviral and cytotoxicity data for compounds **6**–**9** and **2**.

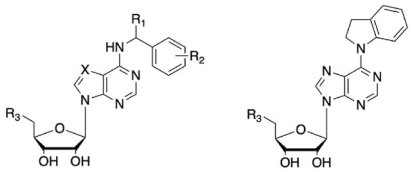

A B

Compound	Scaffold	R_1	R_2	X	R_3	EV71[a]			SARS-CoV-2[b]	ZIKV[c]	Tox.Vero E6
						EC_{50} (μM)[d,e]	*CC_{50} (μM)*[f,e]	*SI*[g]	*EC_{50} (μM)*[d,e]	*EC_{50} (μM)*[d,e]	*CC_{50} (μM)*[f,e]
6a	A	H	3-Cl	N	SMe	0.53 ± 0.40	>20	>37.7	>100	>100	>100
6b	A	H	3-Me	N	SMe	0.898	>75	>83.5	>100	>100	>100
6c	A	H	3-CF_3	N	SMe	>20	>100	n.d.	>100	>100	>100
6d	A	H	3-SF_5	N	SMe	1.85	23.5 ± 8.1	12.7	>100	>100	46.42
6e	A	H	2-Cl	N	SMe	2.61 ± 0.69	>100	>38.3	>100	>100	>100
6f	A	H	4-Cl	N	SMe	8.05 ± 1.70	>100	>12.1	>100	>100	>100
6g	A	Me	3-Cl	N	SMe	4.21 ± 0.93	44.3 ± 19.8	10.5	>100	>100	50.8
6h	A	Me	2-Cl	N	SMe	>100	>100	n.d.	>100	>100	>100
7a	A	H	3-Cl	CH	SMe	>75	>100	n.d.	>100	>100	>100
8	B	–			SMe	19.0	64.9	3.4	>100	>100	>100
9	A	H	3-Cl	N	methyl (2,2,2-trifluoroacetyl)-L-homocysteinate	4.50 ± 1.90	>100	>16.9	>100	>100	>100
11a	A	H	3-Cl	N	OH	0.106 ± 0.037	42.7 ± 3.1	402.8	>100	>100	>100
11b	A	H	3-Me	N	OH	0.094 ± 0.045	>100	>1063	>100	>100	>100
11d	A	H	3-SF_5	N	OH	0.102 ± 0.035	>100	>1282	>100	>100	>100
11e	A	H	2-Cl	N	OH	0.117 ± 0.010	28.2 ± 2.2	241	>100	>100	>100
11f	A	H	4-Cl	N	OH	0.236 ± 0.015	>100	>423.7	>100	>100	>100
11g	A	Me	3-Cl	N	OH	1.07 ± 0.290	>100	>93.5	>100	>100	>100
11h	A	Me	2-Cl	N	OH	>100	>100	n.d.	>100	>100	>100
17	A	H	3-Cl	CH	OH	0.065 ± 0.003	>20	>300.8	>100	>100	>100
19	B	–			OH	>100	>100	n.d.	>100	>100	>100
2	A	H	3-CF_3	N	OH	0.036 ± 0.02	>100	>2770	>100	>100	>100
Rupintrivir [47]	–					0.009 ± 0.001	>1	>111	n.d.	n.d.	n.d.
Remdesivir [50]	–					n.d.			0.058	n.d.	>10
7-DMA [49]	–					n.d.			n.d.	20 ± 15	>300

[a] Antiviral effect on the replication of the EV71 strain BrCr in RD cells.
[b] Antiviral effect on the replication of SARS-CoV-2 ancestral Wuhan strain in Vero E6 cells.
[c] Antiviral effect on the replication of ZIKV strain MR766 in Vero E6 cells.
[d] EC_{50} = 50% effective concentration (concentration at which 50% antiviral effect is observed).
[e] Values are the mean of at least 3 independent experiments, with standard deviations of ±10% of the value quoted unless otherwise stated (mean value ± standard deviations).
[f] CC_{50} = 50% cytotoxic concentration (concentration at which 50% adverse effect is observed on the host cell).
[g] SI = the ratio of CC50 to EC50.

Table 2
Percentage of METTL3/METTL14 activity after 100 μM treatment with the test compounds.

Compound – [100 μM]	METTL3/METTL14 activity (%)	Compound – [100 μM]	METTL3/METTL14 activity (%)
6a	61.67	**11b**	74.45
6d	88.37	**11c**	81.72
6e	68.74	**11d**	82.80
11a	78.23	**17**	35.73
SAH	0.58		

selective anti-EV71 effect in the same range of the parent analogue **17**, without showing the improved antiviral profile that had been anticipated with its design. While the novel phosphoramide prodrug **29** did not show an enhanced antiviral profile compared to the free 5′-OH parent nucleoside analogues **25**, the new pro-nucleotide **27** is associated with an improvement in anti-EV71 activity compared to the parent nucleoside **2**, suggesting that the active form of this compound may indeed be the triphosphate derivative, and it may therefore target the viral polymerase directly as its main mechanism of action. Further investigations to confirm this hypothesis, and to elucidate the reason behind the selectivity of this class of molecules for EV71, are the object

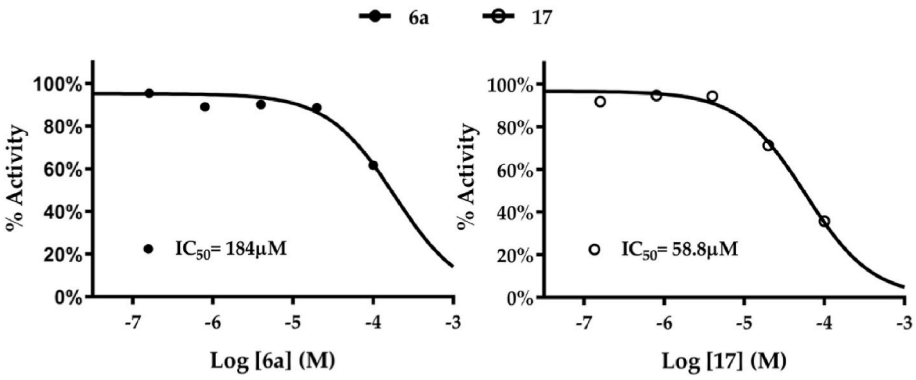

Fig. 7. Dose-response curves and IC_{50} values for **6a** and **17**, obtained from the HotSpot℠ platform for methyltransferases, which measures the residual activity of the METTL3/METTL14 complex in the presence of test compounds.

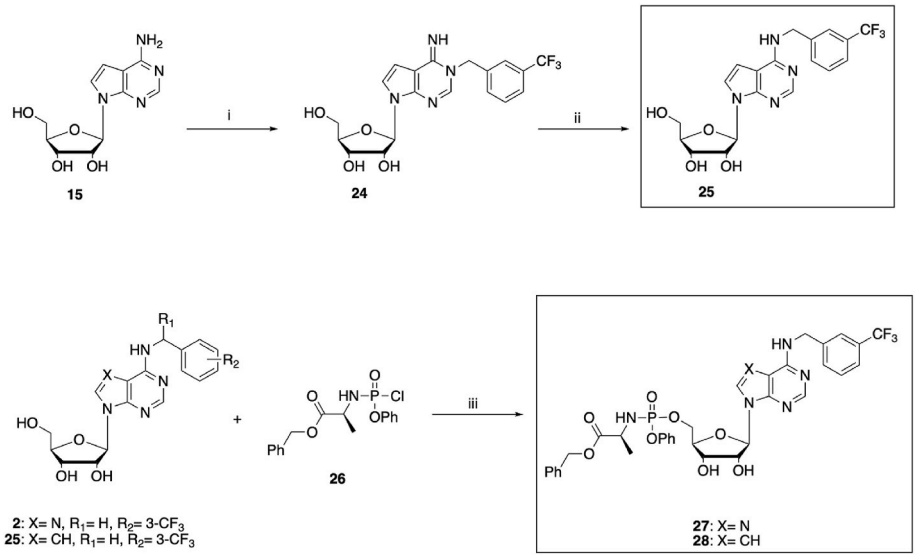

Scheme 3. Synthesis of target compounds **25, 27**–**28**. *Reagents and conditions*: (i) 3-trifluoromethylbenzylbromide, DMF, 75 °C, 24 h; (ii) Me_2NH, THF, MeOH, reflux, o.n. (74% over two steps); (iii) NMI, THF, Pyr, r.t., o.n. (29–36%).

of present investigations.

Despite the boost in antiviral activity observed for **27** versus **2**, both **25** and **27** were still evaluated for their potential direct interference with METTL3 enzymatic activity, using the same assay and conditions reported above. The results obtained for these two additional analogues in the enzymatic assay are shown in Table 4. SAH was used as positive control.

While at least partial inhibition of the METTL3 enzyme was expected for **25**, based on the results obtained for the previous compounds, also the phosphoramidate analogue **27** surprisingly displayed partial inhibition of the activity of the METTL3/METTL14 complex at 100 μM. The inhibitory effect was significantly more prominent for **25**, for which a dose-response curve was calculated, revealing an IC_{50} value in the micromolar range (Fig. 8).

As a final analysis, due to the potent activity found for some of the compounds against the replication of EV71, a selection of these molecules was also evaluated against the replication of a panel of *Enteroviruses* that are currently relevant threats to human health: coxsackievirus B3 (CVB3) in Vero A cells, and coxsackievirus A21 (CVA21), enterovirus 68 (EV68), human rhinovirus A02 (HRV-A02) and human rhinovirus B14 (HRV-B14), all in HeLa cells (Table 5).

All the compounds tested appear to be selective for EV71. The protected, novel 5′-homocysteine analogue **9** displayed a mild antiviral effect against coxsackievirus A21, while both **11b** and **25** displayed antiviral activities against CVA21 and EV68, with an inverted potency profile, and with **11b** showing the lowest EC_{50} values overall. With the exception of **11d**, which showed a cytotoxic effect on HeLa cells at high test concentrations, none of the compounds evaluated displayed any toxicity on the cell models used.

2.5. Structure-activity relationship model

While elucidation of the mechanism of action of the selective antiviral molecules described in this study is the object of current investigations, a structure-activity relationship (SAR) study was performed for compounds **2**, **6**–**9** and **25**, to reveal the structural features responsible for their selective antiviral activity against EV71. For these analyses, the Activity Atlas module in Flare 6.0 was used [55]. Activity Atlas is a qualitative method that identifies distinct structural regions/characteristics shared among the active compounds in a series of analogues, highlighting chemical differences in similar compounds that have an impact on biological activity (known as "activity cliff regions") [56]. The compounds' EC_{50} values against EV71 were used as the reference biological activity to construct the Activity Atlas model. The results obtained show that the most active compounds share a favorable hydrophobic region (green) near the aromatic ring (Fig. 9a, a green area indicates favorable hydrophobic regions). This favorable hydrophobic region is located in proximity of the *meta* position of the

Table 3
Antiviral and cytotoxicity data for compounds **25** and **27**–**28**.

Compound	EV71[a]			SARS-CoV-2[b]	ZIKV[c]	Tox. Vero E6
	EC_{50} (μM)[d,e]	CC_{50} (μM)[f,e]	SI[g]	EC_{50} (μM)[d,e]	EC_{50} (μM)[d,e]	CC_{50} (μM)[f,e]
25	0.101 ± 0.011	>100	>1070	>100	>100	>100
27	0.0169 ± 0.015	9.18	541.9	>100	n.d.	n.d.
28	0.600 ± 0.026	42.5	70.8	>100	n.d.	>100
Rupintrivir [47]	0.009 ± 0.001	>1	>111	n.d.	n.d.	
Remdesivir [50]	n.d.			0.058	n.d.	>10
7-DMA [49]	n.d.			n.d.	20 ± 15	>300

[a] Antiviral effect on the replication of the EV71 strain BrCr in RD cells.
[b] Antiviral effect on the replication of SARS-CoV-2 ancestral Wuhan strain in Vero E6 cells.
[c] Antiviral effect on the replication of ZIKV strain MR766 in Vero E6 cells.
[d] EC_{50} = 50% effective concentration (concentration at which 50% antiviral effect is observed).
[e] Values are the mean of at least 2 independent experiments, with standard deviations of ±10% of the value quoted unless otherwise stated (mean value ± standard deviations).
[f] CC_{50} = 50% cytotoxic concentration (concentration at which 50% adverse effect is observed on the host cell).

Table 4
Percentage of METTL3/METTL14 activity after 100 μM treatment with the two additional test compounds **25** and **27**.

Compound – [100 μM]	METTL3/METTL14 activity (%)	Compound – [100 μM]	METTL3/METTL14 activity (%)
25	56.63	**27**	87.54
SAH	0.58		

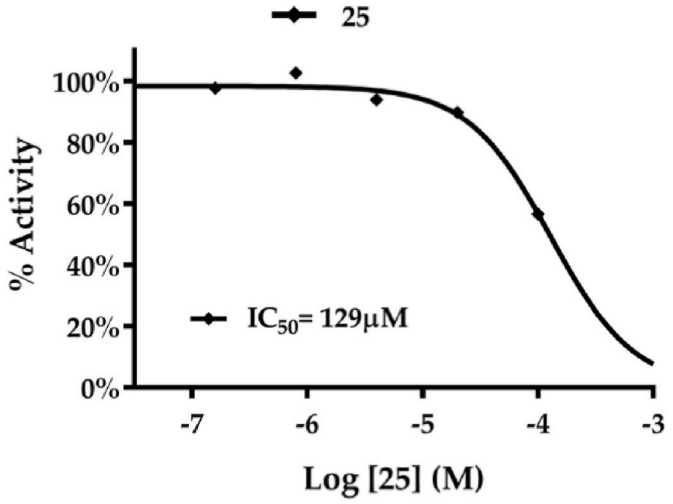

Fig. 8. Dose-response curve and IC_{50} value for **25** obtained from the HotSpot℠ platform for methyltransferases, which measures the residual activity of the METTL3/METTL14 complex in the presence of test compounds.

N-benzyl group. An increased electronegativity in the hydrophobic substituent has contrasting effects for antiviral activity in the 5′-OH and 5′-SMe series of analogues, as it is associated to an increased activity for the trifluoromethyl substituent compared to the methyl for the 5′-OH analogues (**2** vs. **11b**), while it has an opposite effect in the 5′-SMe series (**6c** vs. **6b**). On the contrary, the presence of a hydrophobic group in the proximity of the sugar moiety (5′ position) significantly reduces the antiviral activity of the compounds (Fig. 9a–b, a magenta area indicates an unfavorable hydrophobic region), as evidenced by the fact that the 5′-thiomethyl analogues are all less active than their 5′-hydoxy counterparts (**6a-g** versus **11a-g** and **2**, **7a** versus **17**). The replacement of the 5′-hydroxyl group with the thiomethyl substituent also affects the overall electrostatic features of the molecules (Supplementary Fig. S4), suggesting a different electrostatic complementary between ligands and their target in the two sub-groups of compounds, 5′-hyroxy and 5′-thiomethyl analogues (Fig. 9c).

In order to further explore the observed activity cliffs, we have analyzed the minimal structural modifications that resulted in large variations in anti-EV71 activity using the Activity Miner module in Flare 6.0 [56]. Activity Miner analyses generate different match molecular pairs (MPPs), evaluating a "disparity value", which correlates the similarity between a pair of molecules with the difference in their biological activity in a given assay (Disparity Value = ΔActivity/(1-Similarity)). These MMPs analyses revealed that introduction of a methyl group at the benzylic position, between the adenine core and the phenyl ring, has a significant effect on anti-EV71 activity, drastically reducing the antiviral effect of the corresponding analogue (Fig. 9d, compound **11a** vs **11b**), possibly due to steric hindrance of the methyl group. On the contrary, the replacement of the *meta* chloro-substituent a trifluoromethyl is associated with a significant increase in antiviral activity against EV71 for the 5′-OH series of compounds, possibly due to an optimal combination of both electrostatics (hydrophobic, electronegative substituent) and occupational volume. Considering these observations, further structural modifications may explore the electron withdrawing effect (EWG) of different substituents on the aromatic ring, introducing further EWG groups such as OCF_3, CN, SO_2NH_2, and polar hydrophilic groups in the proximity of the sugar moiety (e.g., replacing the hydroxyl group with a more polar amine group, NH_2).

3. Conclusions

In this work, a series of novel nucleoside analogues were rationally designed as potential inhibitors of the METTL3 methyltransferase, as a novel approach to interfere with the replication of different viruses. After their ability to bind to the SAM pocket of the METTL3 crystal structure was confirmed by molecular docking studies, the newly designed small molecules were synthesized according to two-to six-step synthetic routes. Twenty-four compounds were evaluated for their ability to interfere with the replication of different viruses in cell-based assays, with several displaying selective inhibition of EV71 replication with EC_{50} values in the sub-micromolar range. A selection of compounds was also evaluated for their direct inhibition of METTL3 activity *in vitro*, with three small molecules displaying IC_{50} values in the micromolar range. The higher IC_{50}s observed in the enzymatic assay compared to the EC_{50}s obtained in the anti-EV71 assay appear to indicate that inhibition of human METLL3 is not the main mechanism of action for these compounds. Considering that their main target may be a viral protein, and due to the fact that in most cases antiviral nucleoside analogues act by inhibiting the viral polymerase in their triphosphate active form, a small series of novel phosphoramidate prodrugs of some of the best anti-EV71 candidates identified was synthesized. The phosphoramidate prodrug technique enables a fast activation of nucleoside analogues to their triphosphate active species in cells, and this approach revealed potent inhibitors of EV71 replication. On top of further indicating that the main target for the action of this antiviral scaffold may be the viral polymerase, these potent analogues provide suitable candidates for further, future studies in pre-clinical models. The aim of additional studies currently being carried out is also to address the marked selectivity of this class of antiviral agents for EV71, the reason for which has not been elucidated yet. Finally, although the antiviral activity of the compounds is likely to be mainly due to interference with a different target

Table 5
Antiviral and cytotoxicity data for selected compounds against a panel of enteroviruses.

Compound	CVB3[a]		CVA21[b]	EV68[b]	HRV-A02[b]	HRV-B14[b]	Tox in HeLa cells
	EC_{50} (μM)[c,d]	CC_{50} (μM)[e,d]	EC_{50} (μM)[c,d]	EC_{50} (μM)[c,d]	EC_{50} (μM)[c,d]	EC_{50} (μM)[c,d]	CC_{50} (μM)[e,d]
6b	>100	>50	>100	>100	>100	>100	>100
9	>100	>100	54.6	>100	>100	>100	>100
11b	>100	>100	36.4	8.9	>100	>100	>100
11d	>100	>100	31.7	>100	>100	>100	88.7
11g	>100	>100	>100	>100	>100	>100	>100
25	>100	>100	19.9	91.2	>100	>100	>100

[a] Antiviral effect on the replication of CoxB3 in Vero A cells.
[b] Antiviral effect on viral replication in HeLa cells.
[c] EC_{50} = 50% effective concentration (concentration at which 50% antiviral effect is observed).
[d] Values are the mean of at least 2 independent experiments.
[e] CC_{50} = 50% cytotoxic concentration (concentration at which 50% adverse effect is observed on the host cell).

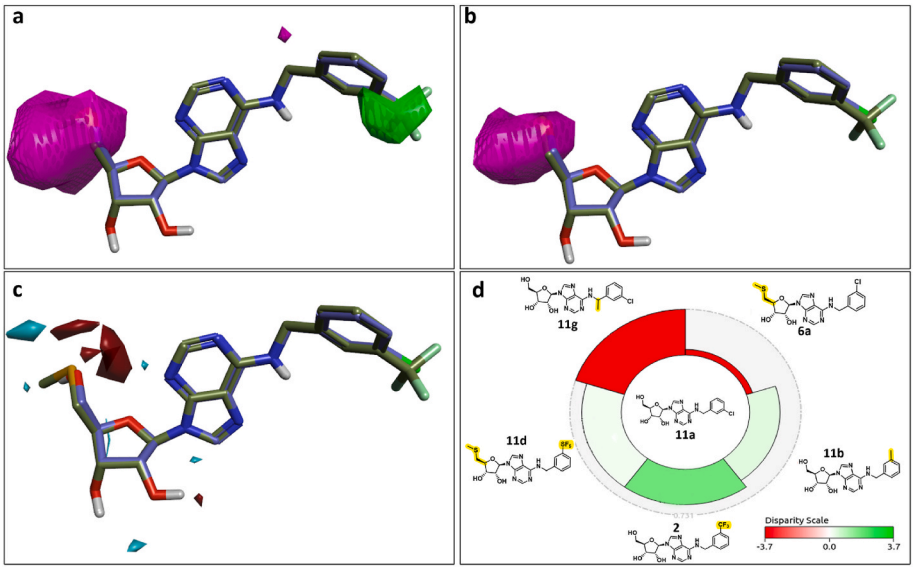

Fig. 9. Activity Atlas analysis revealing key features of the test compounds that influence their anti-EV71 activity. a, b) Activity cliff analysis reveals a favorable hydrophobic region (green) and an unfavorable hydrophobic region (magenta). c) Negative (red) and positive (cyan) electrostatic regions. d) MMP analyses between **11a** and its analogues (**2**, **6a**, **11b, 11d** and **11g**). The size of the segment shows the structural similarity (FCFP6) between a pair of molecules, smaller segments indicate higher structural similarity. The colours indicate the disparity value (green: increase of antiviral activity; red: decrease of antiviral activity).

fundamental to EV71 replication, possibly the viral polymerase as indirectly suggested by the antiviral effect observed for the phosphoramidate analogues, some of these molecules still show the potential to inhibit the activity of human METTL3 in the micromolar range. They therefore represent suitable candidates for further structural modifications, aimed at optimizing their potencies as inhibitors of this enzyme for antiviral purposes. To the best of our knowledge, the molecules discussed in this study represent the first example of antiviral agents showing METLL3 inhibitory activity, and our results so far appear to support the feasibility of targeting the METTL3/METTL14 complex for developing new antiviral therapeutics.

4. Materials and methods

4.1. Molecular modelling studies

All molecular modelling experiments were performed on Asus WS X299 PRO Intel® i9-10980XE CPU @ 3.00 GHz × 36 running Ubuntu 18.04 (graphic card: GeForce RTX 2080 Ti). Molecular Operating Environment (MOE) 2019.10 [57] and Maestro (Schrödinger Release 2020-2) [41] were used as molecular modelling software. The structures of the newly designed compounds were built in MOE, saved in.sdf format and prepared using the Maestro LigPrep tool by energy minimising the structures (OPLS_2005 force filed), generating possible ionization states at pH 7 ± 2, generating tautomers, generating all possible stereoisomers per ligand and low-energy ring conformers.

The crystal structure of METTL3 in complex with SAM was downloaded from the PDB (http://www.rcsb.org/; PDB code 5IL1). The protein was prepared using the MOE Protein Preparation tools, and the resulting protein-ligand complex was saved in.mae format to be used in Maestro for the docking simulations. The protein in.mae format was preprocessed using the Schrödinger Protein Preparation Wizard by assigning bond orders, adding hydrogens and performing a restrained energy minimization of the added hydrogens using the OPLS_2005 force field. A 9 Å docking grid (inner-box 10 Å and outer-box 19 Å) was prepared using as centroid the co-crystallised SAM. The docking analyses were performed using Glide SP precision keeping the default parameters and setting as 25 the number of output poses per input ligand to include in the solution, performing for each pose a post-docking minimization. The docking results were then visually inspected using MOE 2019.10.

The Activity-Atlas models were constructed using Flare 6.0 [55]. First, a pharmacophore model was generated by comparing the electrostatic and hydrophobic properties of **6a**, **11a** and **11b**. Then the molecular structures of each compound were subjected to a field-based alignment to the pharmacophore according to common electrostatic and hydrophobic distributions between each compound and the pharmacophore model. After the alignment, the SAR model was constructed by correlating the field point-based descriptors and the corresponding EV71 antiviral EC_{50} values (pEC_{50}) of each compound. The Activity miner module (Flare 6.0) was used to compare the different MMPS and acquire information on the field and steric contributions significant for the activity.

4.2. Synthetic chemistry

All solvents and reagents were used as obtained from commercial sources unless otherwise indicated. All solvents used for chromatography were HPLC grade from Fisher Scientific (UK). All reactions were performed under a nitrogen atmosphere. ^{1}H, ^{13}C, ^{19}F and ^{31}P NMR spectra were recorded with a Bruker Avance III HD spectrometer operating at 500 MHz for ^{1}H and 125 MHz for ^{13}C, with Me_4Si as internal standard. Deuterated chloroform or dimethylsulfoxide were used as the solvents for NMR experiments, unless otherwise stated. ^{1}H chemical shifts values (δ) are referenced to the residual non-deuterated components of the NMR solvents (δ = 7.26 ppm for $CHCl_3$, etc.). The ^{13}C chemical shifts (δ) are referenced to $CDCl_3$ (central peak, δ = 77.0 ppm). TLC was performed on silica gel 60 F254 plastic sheets. Flash column chromatography was performed using a Biotage Isolera One automated system. UPLC-MS analysis was conducted on a Waters UPLC system with both Diode Array detection and Electrospray (+′ve and −′ve ion) MS detection. The stationary phase was a Waters Acquity UPLC BEH C18 1.7 μm 2.1 50 mm column. The mobile phase was LC-MS grade H_2O containing 0.1% formic acid (A) and LC-MS grade MeCN containing 0.1% formic acid (B). Column temperature: 40 °C. Sample diluent: MeCN. Sample concentration: 1 μg/mL. Injection volume: 2 μL. Three alternative methods were used: Linear gradient standard method (A): 90% A (0.1 min), 90–0% A (2.5 min), 0% A (0.3 min), 90% A (0.1 min); flow rate 0.5 mL/min. Linear gradient standard method (B): 90% A (0.1 min), 90–0% A (2.1 min), 0% A (0.8 min), 90% A (0.1 min); flow rate 0.5 mL/min. Linear gradient standard method (C): 90% A (0.1 min), 90–0% A (1.5 min), 0% A (1.4 min), 90% A (0.1 min); flow rate 0.5 mL/min. High resolution mass spectra (HRMS) were measured in positive mode electrospray ionization (ES+). All compounds tested in biological assays were >95% pure. Purity of intermediates that were not biologically evaluated was >90%, unless otherwise stated. Preparation and characterization of all intermediates are fully described in the Supporting *Information*, while details for the preparation of the final target products **6**–**9**, **25** and **27**–**28** are given below.

4.2.1. General procedure for the preparation of 5′-thiomethyl ribofuranosides *6a-c*

The appropriate N^6-benzyl adenosine analogue **2**, **11a-b** (0.8 mmol, 1 eq.) was added to 3 mL of anhydrous DMF, followed by methyl disulphide (3.8 mmol, 5 eq.) and tributylphosphine (3.8 mmol, 5 eq.). The reaction was stirred at room temperature under nitrogen atmosphere for 48 h, then quenched by addition of deionised water (10 mL) and stirred at room temperature for further 10 min. The reaction was concentrated to dryness under vacuum, and the crude reside was purified by automated flash column chromatography eluting with *n*-hexane-DCM-MeOH 100:0:0 v/v increasing to *n*-hexane-DCM-MeOH 0:85:15 v/v in 20 CV.

- (2*R*,3*R*,4*S*,5*S*)-2-(6-((3-Chlorobenzyl)amino)-9*H*-purin-9-yl)-5-((methylthio)methyl)tetrahydrofuran-3,4-diol **6a**

Obtained as a white solid in 57% yield. ^{1}H NMR (DMSO-d_6), δ: 8.46 (bs, 1H, NH), 8.41 (s, 1H), 8.24 (s, 1H), 7.39 (s, 1H), 7.35–7.27 (m, 3H), 6.92 (d, J = 5.4 Hz, 1H, H-1′), 5.49 (bs, 1H, 2′-OH), 5.32 (bs, 1H, 3′-OH), 4.78–4.71 (m, 3H), 4.16 (m, 1H, H-3′), 4.05 (m, 1H, H-4′), 2.88 (dd, J_1 = 13.5 Hz, J_2 = 5.7 Hz, 1H, H-5′), 2.79 (dd, J_1 = 13.5 Hz, J_2 = 5.7 Hz, 1H, H-5′), 2.06 (s, 3H). ^{13}C NMR (DMSO-d_6), δ: 154.7, 153.0, 143.2, 140.5, 133.3, 130.6, 127.5, 127.3, 127.0, 126.2, 120.1, 87.9, 84.2, 73.1, 73.0, 42.9, 36.5, 16.0. UPLC-MS (Method A): t_R 1.98 min, MS [ESI, *m/z*]: 422.2, 424.2 [M+H$^+$]. HRMS calculated for $C_{18}H_{21}ClN_5O_3S^+$: 422.1048; found 422.1051.

- (2*R*,3*R*,4*S*,5*S*)-2-(6-((3-Methylbenzyl)amino)-9*H*-purin-9-yl)-5-((methylthio)methyl)tetrahydrofuran-3,4-diol **6b**

Obtained as a white solid in 51% yield. ^{1}H NMR (DMSO-d_6), δ: 8.39 (s, 1H), 8.36 (bs, 1H, NH), 8.22 (s, 1H), 7.19–7.12 (m, 3H), 7.02 (d, J = 7.2 Hz, 1H), 5.91 (d, J = 5.6 Hz, 1H, H-1′), 5.50 (bs, 1H, 2′-OH), 5.32 (bs, 1H, 3′-OH), 4.76 (m, 1H, H-2′), 4.68 (bs, 2H), 4.16 (m, 1H, H-3′), 4.04 (m, 1H, H-4′), 2.89 (dd, J_1 = 14.2 Hz, J_2 = 5.5 Hz, 1H, H-5′), 2.79 (dd, J_1 = 14.2 Hz, J_2 = 5.5 Hz, 1H, H-5′), 2.26 (s, 3H), 2.06 (s, 3H). ^{13}C NMR (DMSO-d_6), δ: 154.5, 153.0, 145.4, 137.6, 130.6, 128.5, 128.1, 127.7, 124.6, 120.9, 87.9, 84.2, 73.1, 73.0, 42.8, 36.5, 21.5, 16.0. UPLC-MS (Method A): t_R 1.91 min, MS [ESI, *m/z*]: 402.3 [M+H$^+$]. HRMS calculated for $C_{19}H_{24}N_5O_3S^+$: 402.1594; found 402.1600.

- (2*S*,3*S*,4*R*,5*R*)-2-((Methylthio)methyl)-5-(6-((3-(trifluoromethyl)benzyl)amino)-9*H*-purin-9-yl)tetrahydrofuran-3,4-diol **6c**

Obtained as a white solid in 40% yield. ^{1}H NMR (DMSO-d_6), δ: 8.52 (bs, 1H, NH), 8.41 (s, 1H), 8.24 (s, 1H), 7.72 (s, 1H), 7.66 (d, J = 6.7 Hz, 1H), 7.60–7.53 (m, 2H), 5.91 (d, J = 5.6 Hz, 1H, H-1′), 5.49 (d, J = 4.8 Hz, 1H, 2′-OH), 5.32 (d, J = 4.3 Hz, 1H, 3′-OH), 4.83–4.74 (m, 3H), 4.16 (m, 1H, H-3′), 4.04 (m, 1H, H-4′), 2.89 (dd, J_1 = 13.9 Hz, J_2 = 5.6 Hz, 1H, H-5′), 2.79 (dd, J_1 = 13.9 Hz, J_2 = 5.6 Hz, 1H, H-5′), 2.06 (s, 3H). ^{19}F NMR (DMSO-d_6), δ: 61.01. ^{13}C NMR (DMSO-d_6), δ: 154.8, 153.0, 142.0, 140.5, 131.7, 129.7, 129.5 (m), 125.8, 124.1 (m), 123.8 (m), 103.3 (m), 99.9, 87.9, 84.2, 73.1, 73.0, 43.0, 36.5, 16.0. UPLC-MS (Method A): t_R 2.08 min, MS [ESI, *m/z*]: 456.2 [M+H$^+$]. HRMS calculated for $C_{19}H_{21}F_3N_5O_3S^+$: 456.1312; found 456.1303.

4.2.2. General procedure for the preparation of 5′-thiomethyl ribofuranosides *6d-h, 8*

The appropriate N^6-substituted adenosine 5′-chloride analogue **11d-h**, **20** (0.5 mmol, 1 eq.) and sodium thiomethoxide (1.0 mmol, 2 eq.) were dissolved in 3 mL of anhydrous DMF under nitrogen atmosphere. The reaction was stirred at room temperature overnight, then the residue was concentrated to dryness under *vacuum*. The crude reside was purified by automated flash column chromatography eluting with *n*-hexane-DCM-MeOH 100:0:0 v/v increasing to *n*-hexane-DCM-MeOH 0:80:20 v/v in 15 CV.

- (2*S*,3*S*,4*R*,5*R*)-2-((Methylthio)methyl)-5-(6-((3-(pentafluorosulfanyl)benzyl)amino)-9*H*-purin-9-yl)tetrahydrofuran-3,4-diol **6d**

Obtained as a white solid in 81% yield. ^{1}H NMR (DMSO-d_6), δ: 8.55 (bs, 1H, NH), 8.42 (s, 1H), 8.24 (s, 1H), 7.91 (s, 1H), 7.76 (d, J = 7.6 Hz, 1H), 7.64 (d, J = 7.6 Hz, 1H), 7.55 (app t, J = 7.6 Hz, 1H), 5.91 (d, J = 5.6 Hz, 1H, H-1′), 5.50 (d, J = 5.8 Hz, 1H, 2′-OH), 5.32 (d, J = 5.0 Hz, 1H, 3′-OH), 4.84–4.74 (m, 3H), 4.16 (m, 1H, H-3′), 4.04 (m, 1H, H-4′), 2.88 (dd, J_1 = 13.9 Hz, J_2 = 5.8 Hz, 1H, H-5′), 2.78 (dd, J_1 = 13.9 Hz, J_2 = 5.8 Hz, 1H, H-5′), 2.06 (s, 3H). ^{19}F NMR (DMSO-d_6), δ: 87.6 (quintet, J = 149.7, 1F), 63. 9 (d, J = 149.7, 4F). ^{13}C NMR (DMSO-d_6), δ: 154.6, 153.4, 153.0, 142.4, 140.6, 131.7, 129.8, 124.9 (m), 124.5 (m), 120.0 (m), 116.8, 87.9, 84.2, 73.1, 73.0, 43.1, 36.5, 16.0. UPLC-MS (Method A): t_R 2.17 min, MS [ESI, *m/z*]: 514.1 [M+H$^+$]. HRMS calculated for $C_{18}H_{21}F_5N_5O_3S_2^+$: 514.1000; found 514.0993.

- (2*R*,3*R*,4*S*,5*S*)-2-(6-((2-Chlorobenzyl)amino)-9*H*-purin-9-yl)-5-((methylthio)methyl)tetrahydrofuran-3,4-diol **6e**

Obtained as a white solid in 74% yield. ^{1}H NMR (DMSO-d_6), δ: 8.43 (s, 1H), 8.42 (bs, 1H, NH), 8.22 (s, 1H), 7.46–7.44 (m, 1H), 7.28–7.25 (m, 3H), 5.92 (d, J = 5.8 Hz, 1H, H-1′), 5.50 (d, J = 5.7 Hz, 1H, 2′-OH), 5.33 (d, J = 4.8 Hz, 3′-OH), 4.77 (bs, 3H), 4.16 (m, 1H, H-3′), 4.04 (m, 1H, H-4′), 2.89 (dd, J_1 = 13.6 Hz, J_2 = 5.7 Hz, 1H, H-5′), 2.79 (dd, J_1 = 13.6 Hz, J_2 = 5.7 Hz, 1H, H-5′), 2.07 (s, 3H). ^{13}C NMR (DMSO-d_6), δ: 154.7, 153.0, 148.9, 145.2, 140.6, 137.2, 132.1, 129.5, 128.7, 128.3, 127.5, 87.9, 84.2, 73.1, 73.0, 41.4, 36.5, 16.0. UPLC-MS (Method A): t_R 1.96 min, MS [ESI, *m/z*]: 422.2, 424.2 [M+H$^+$]. HRMS calculated for

$C_{18}H_{21}ClN_5O_3S^+$: 422.1048; found 422.1039.

- (2*R*,3*R*,4*S*,5*S*)-2-(6-((4-Chlorobenzyl)amino)-9*H*-purin-9-yl)-5-((methylthio)methyl)tetrahydrofuran-3,4-diol **6f**

Obtained as a white solid in 59% yield. ^{1}H NMR (DMSO-d_6), δ: 8.45 (bs, 1H, NH), 8.40 (s, 1H), 8.22 (s, 1H), 7.36 (s, 4H), 5.91 (d, J = 5.7 Hz, 1H, H-1′), 5.49 (d, J = 5.6 Hz, 1H, 2′-OH), 5.32 (d, J = 4.4 Hz, 3′-OH), 4.76 (m, 1H, H-2′), 4.69 (bs, 2H), 4.16 (m, 1H, H-3′), 4.04 (m, 1H, H-4′), 2.88 (dd, J_1 = 12.9 Hz, J_2 = 5.8 Hz, 1H, H-5′), 2.79 (dd, J_1 = 12.9 Hz, J_2 = 5.8 Hz, 1H, H-5′), 2.06 (s, 3H). ^{13}C NMR (DMSO-d_6), δ: 154.4, 153.0, 143.7, 140.4, 139.6, 135.9, 131.6, 129.4, 128.6, 87.9, 84.2, 73.1, 73.0, 42.7, 36.5, 16.0. UPLC-MS (Method A): t_R 1.98 min, MS [ESI, *m/z*]: 422.2, 424.2 [M+H$^+$]. HRMS calculated for $C_{18}H_{21}ClN_5O_3S^+$: 422.1048; found 422.1052.

- (2*R*,3*R*,4*S*,5*S*)-2-(6-((1-(3-Chlorophenyl)ethyl)amino)-9*H*-purin-9-yl)-5-((methylthio)methyl)tetrahydrofuran-3,4-diol **6g**

Obtained as a white solid in 64% yield. ^{1}H NMR (DSMO-d_6), δ: 8.44–8.33 (m, 4H), 8.20 (m, 2H), 7.52 (s, 2H), 7.42–7.38 (m, 2H), 7.35–7.30 (m, 2H), 7.27–7.23 (m, 2H), 5.91 (d, J = 5.9 Hz, 1H, H-1′), 5.89 (d, J = 6.0 Hz, 1H, H-1′), 5.53–5.47 (m, 2H), 4.78–4.72 (m, 2H, H-2′), 4.17–4.13 (m, 2H, H-3′), 4.05–4.01 (m, 2H, H-4′), 2.90–2.86 (m, 2H, H-5′), 2.81–2.76 (m, 2H, H-5'), 2.06 (s, 6H), 1.53 (d, J = 6.2 Hz, 6H). ^{13}C NMR (DSMO-d_6), δ: 154.1, 152.8, 147.2, 139.9, 133.3, 130.5, 126.9, 126.4, 125.4, 112.5, 87.8, 84.2, 84.1, 73.1, 73.0, 36.5, 21.3, 16.0. UPLC-MS (Method B): t_R 1.91 min, MS [ESI, *m/z*]: 436.2, 438.2 [M+H$^+$]. HRMS calculated for $C_{19}H_{23}ClN_5O_3S^+$: 436.1205; found 436.1198.

- (2*R*,3*R*,4*S*,5*S*)-2-(6-((1-(2-Chlorophenyl)ethyl)amino)-9*H*-purin-9-yl)-5-((methylthio)methyl)tetrahydrofuran-3,4-diol **6h**

Obtained as a white solid in 72% yield. ^{1}H NMR (DMSO-d_6), δ: 8.54 (bs, 2H), 8.47 (s, 2H), 8.23 (s, 2H), 7.65–7.60 (m, 2H), 7.48–7.44 (m, 2H), 7.35–7.25 (m, 4H), 5.98–5.94 (m, 2H, H-1′), 5.82 (bs, 2H), 5.55 (d, J = 5.6 Hz, 2H, 2′-OH), 5.37 (d, J = 4.8 Hz, 2H, 3′-OH), 4.83–4.79 (m, 2H, H-2′), 4.24–4.18 (m, 2H, H-3′), 4.11–4.06 (m, 2H, H-4′), 2.94–2.90 (m, 2H, H-5′), 2.87–2.81 (m, 2H, H-5′), 2.11 (s, 6H), 1.57 (d, J = 6.3 Hz, 6H). ^{13}C NMR (DSMO-d_6), δ: 154.1, 152.9, 149.0, 143.1, 140.3, 132.0, 129.7, 128.6, 127.8, 127.3, 115.2, 87.8, 84.2, 84.1, 73.1, 73.0, 36.5, 21.5, 16.0. UPLC-MS (Method B): t_R 1.95 min, MS [ESI, *m/z*]: 436.2, 438.2 [M+H$^+$]. HRMS calculated for $C_{19}H_{23}ClN_5O_3S^+$: 436.1205; found 436.1203.

- (2*R*,3*R*,4*S*,5*S*)-2-(6-(Indolin-1-yl)-9*H*-purin-9-yl)-5-((methylthio) methyl)tetrahydrofuran-3,4-diol **8**

Obtained as a white solid in 72% yield. ^{1}H NMR (DMSO-d_6), δ: 8.63 (d, J = 8.0 Hz, 1H), 8.54 (s, 1H), 8.50 (s, 1H), 7.30 (d, J = 7.3 Hz, 1H), 7.23 (app t, J = 7.3 Hz, 1H), 7.03–6.99 (m, 1H), 6.00 (d, J = 5.6 Hz, 1H, H-1′), 5.55 (d, J = 5.7 Hz, 1H, 2′-OH), 5.36 (d, J = 5.0 Hz, 1H, 3′-OH), 4.81–4.76 (m, 3H), 4.18 (m, 1H, H-3′), 4.06 (m, 1H, H-4′), 3.29–3.26 (m, 2H), 2.91 (dd, J_1 = 13.1 Hz, J_2 = 5.7 Hz, 1H, H-5′), 2.81 (dd, J_1 = 13.1 Hz, J_2 = 5.7 Hz, 1H, H-5′), 2.08 (s, 3H). ^{13}C NMR (DMSO-d_6), δ: 152.1, 151.7, 151.5, 144.1, 140.5, 132.6, 127.3, 125.2, 123.1, 120.8, 117.3, 87.7, 84.2, 73.2, 73.0, 51.2, 36.5, 28.2, 16.0. UPLC-MS (Method B): t_R 1.98 min, MS [ESI, *m/z*]: 400.2 [M+H$^+$]. HRMS calculated for $C_{19}H_{22}N_5O_3S^+$: 400.1438; found 400.1441.

*4.2.3. Synthesis of (2R,3R,4S,5S)-2-(4-((3-chlorobenzyl)amino)-7H-pyrrolo[2,3-d]pyrimidin-7-yl)-5-((methylthio)methyl)tetrahydrofuran-3,4-diol **7a***

7-Deaza-adenosine 5′-chloride analogue **18** (0.15 mmol, 1 eq.) and sodium thiomethoxide (0.30 mmol, 2 eq.) were dissolved in 2 mL of anhydrous DMF under nitrogen atmosphere. The reaction was stirred at room temperature overnight, then the residue was concentrated to dryness under *vacuum*. The crude reside was purified by automated flash column chromatography eluting with *n*-hexane-EtOAc 100:0:0 v/v increasing to *n*-hexane-EtOAc 0:100 v/v in 15 CV to give the title compound as a white solid in 43% yield. ^{1}H NMR ($CDCl_3$), δ: 8.16 (s, 1H), 7.16 (m, 4H), 7.12 (d, J = 3.1 Hz, 1H), 6.61 (bs, 1H, NH), 6.23 (d, J = 3.1 Hz, 1H), 5.92 (d, J = 5.5 Hz, 1H, H-1′), 5.29 (bs, 1H, 2′-OH), 4.76–4.68 (m, 2H), 4.37 (app t, J = 5.5 Hz, 1H, H-2′), 4.31 (m, 1H, H-4′), 4.24 (m, 1H, H-3′), 3.40 (bs, 1H, 3′-OH), 2.71 (d, J = 5.8 Hz, 2H, H-5′), 2.08 (s, 3H). ^{13}C NMR ($CDCl_3$), δ: 156.2, 151.3, 143.9, 140.7, 131.0, 130.0, 127.7, 127.6, 125.6, 122.1, 108.6, 97.8, 90.6, 84.7, 75.9, 73.9, 37.0, 29.7, 16.6. UPLC-MS (Method A): t_R 1.82 min, MS [ESI, *m/z*]: 421.2, 423.2 [M+H$^+$]. HRMS calculated for $C_{19}H_{22}ClN_4O_3S^+$: 421.1096; found 421.1201.

*4.2.4. Synthesis of methyl S-(((2S,3S,4R,5R)-5-(6-((3-chlorobenzyl) amino)-9H-purin-9-yl)-3,4-dihydroxytetrahydrofuran-2-yl)methyl)-N-(2,2,2-trifluoroacetyl)-L-homocysteinate **9***

The functionalised N^6-benzyl adenosine analogue **11a** (0.5 mmol, 1 eq.) was added to 2 mL of anhydrous DMF, followed by fully protected *L*-homocystine 23 (1.5 mmol, 3 eq.) and tributylphosphine (3.0 mmol, 6 eq.). The reaction was stirred at room temperature under nitrogen atmosphere for 48 h, then quenched by addition of deionised water (7 mL) and stirred at room temperature for further 10 min. The reaction was concentrated to dryness under vacuum, and the crude reside was purified by automated flash column chromatography eluting with *n*-hexane-EtOAc 100:0 v/v increasing to *n*-hexane-EtOAc 0:100 v/v in 15 CV to give the title compound as a white solid in 21% yield. ^{1}H NMR ($CDCl_3$), δ: 8.30 (s, 1H), 7.94 (s, 1H), 7.39–7.35 (m, 2H), 7.23 (s, 2H), 6.49 (bs, 1H, NH), 6.11 (bs, 1H, NH), 5.90 (d, J = 4.8 Hz, 1H, H-1'), 4.83 (bs, 2H), 4.76–4.72 (m, 1H), 4.60 (m, 1H), 4.37 (m, 2H), 3.79 (m, 1H), 3.76 (s, 3H), 2.85 (m, 2H), 2.61 (t, J = 6.8 Hz, 2H), 2.21–2.16 (m, 1H), 2.06–2.00 (m, 2H). ^{19}F NMR ($CDCl_3$), δ: 75.7. ^{13}C NMR ($CDCl_3$), δ: 170.7, 162.9, 154.8, 152.7, 140.4, 138.3, 134.5, 131.5, 129.9, 127.7, 127.7, 125.7, 117.3, 114.0, 90.3, 85.1, 75.2, 73.3, 53.1, 34.7, 31.5, 30.3, 28.6. UPLC-MS (Method A): t_R 2.17 min, MS [ESI, *m/z*]: 619.2, 621.2 [M+H$^+$]. HRMS calculated for $C_{24}H_{27}ClF_3N_6O_6S^+$: 619.1348; found 619.1359.

*4.2.5. Synthesis of (2R,3S,4R,5R)-2-(hydroxymethyl)-5-(4-((3-(trifluoromethyl)benzyl)amino)-7H-pyrrolo[2,3-d]pyrimidin-7-yl) tetrahydrofuran-3,4-diol **25***

3-Trifluoromethylbenzyl bromide (0.56 mmol, 3 eq.) was added to a stirred solution of tubercidin **15** (0.19 mmol, 1 eq.) in 1 mL of anhydrous DMF under nitrogen atmosphere. The reaction was stirred at 75 °C for 24 h, and then dried under vacuum. The crude residue was purified by automated flash column chromatography eluting with *n*-hexane-DCM-MeOH 100:0: v/v increasing to *n*-hexane-DCM-MeOH 0:85:15 v/v in 23 CV to give the structural isomer **24** as a sticky glue in quantitative yield. **24** was then dissolved in MeOH (2 mL), a 2 M solution of dimethylamine in THF (1.5 mL) was added, and the solution was heated to reflux while stirring overnight. The reaction was then dried under *vacuum*, and the crude residue was purified by automated flash column chromatography eluting with *n*-hexane-DCM-MeOH 100:0: v/v increasing to *n*-hexane-DCM-MeOH 0:85:15 v/v in 20 CV to afford the title compound as a white solid in 74% yield over two steps. ^{1}H NMR (DMSO-d_6), δ: 8.19 (t, J = 6.1 Hz, 1H, NH), 8.13 (s, 1H), 7.69 (s, 1H), 7.65–7.63 (m, 1H), 7.61–7.59 (m, 1H), 7.57–7.54 (m, 1H), 7.39 (d, J = 3.6 Hz, 1H), 6.66 (d, J = 3.6 Hz, 1H), 6.02 (d, J = 6.2 Hz, 1H, H-1′), 5.27–5.23 (m, 2H, 2′-OH, 5′-OH), 5.10 (d, J = 4.7 Hz, 1H, 3′-OH), 4.82–4.80 (m, 2H), 4.45–4.41 (m, 1H, H-2′), 4.11–4.06 (m, 1H, H-3′), 3.89–3.88 (m, 1H, H-4′), 3.64–3.61 (m, 1H, H-5′), 3.55–3.51 (m, 1H, H-5′). ^{19}F NMR (DMSO-d_6), δ: 61.0. ^{13}C NMR (DMSO-d_6), δ: 156.4, 151.7, 149.9, 142.2, 131.7, 129.8, 129.3 (m), 125.8, 124.0 (m), 123.9 (m), 123.0, 116.4 (m), 103.9, 99.6, 87.9, 85.5, 74.2, 71.1, 62.2, 43.1. UPLC-MS (Method A): t_R 1.76 min, MS [ESI, *m/z*]: 425.3 [M+H$^+$]. HRMS calculated for $C_{19}H_{20}F_3N_4O_4^+$: 425.1431; found

425.1429.

*4.2.6. General procedure for the preparation of phosphoramidates **27–28***

The appropriate ribofuranoside **4**, **11g** or **25** (1 mmol, 1 eq.) was suspended in 8 mL of anhydrous Pyr and 4 mL of anhydrous THF under N_2 atmosphere. NMI (6 mmol, 6 eq.) was added and the reaction was stirred at room temperature for 20 min. Benzyl (chloro(phenoxy)phosphoryl)-L-alaninate **26** (1.5 mmol, 1.5 eq.) was dissolved in 8 mL of anhydrous THF under N_2 atmosphere and added to the mixture, which was then stirred at room temperature overnight. The reaction mixture was then concentrated under *vacuum*, and the crude reside was purified by automated flash column chromatography eluting with DCM-MeOH 100:0:0 v/v increasing to DCM-MeOH 90:10 v/v in 15 CV.

- Benzyl ((((2R,3S,4R,5R)-3,4-dihydroxy-5-(6-((3-(trifluoromethyl)benzyl)amino)-9*H*-purin-9-yl)tetrahydrofuran-2-yl)methoxy)(phenoxy)phosphoryl)-L-alaninate **27**

Obtained as a white sticky solid in 29% yield (diastereomeric mixture with the two diastereomers in a 1:1 ratio). ^{1}H NMR ($CDCl_3$), δ: 8.31 (s, 2H), 7.97 (s, 1H), 7.94 (s, 1H), 7.63 (s, 2H), 7.56–7.51 (m, 4H), 7.43–7.40 (m, 2H), 7.34–7.27 (m, 10H), 7.17–7.12 (m, 4H), 7.07–7.04 (m, 5H), 7.00–6.97 (m, 1H), 6.41 (bs, 2H), 5.92 (d, J = 5.4 Hz, 1H, H-1′), 5.90 (d, J = 5.2 Hz, 1H, H-1′), 5.10–5.06 (m, 4H), 4.89 (bs, 4H), 4.41–4.24 (m, 9H), 4.22–4.17 (m, 1H), 4.10–3.93 (m, 4H, H-5'), 1.30 (d, J = 4.0 Hz, 3H), 1.29 (d, J = 3.9 Hz, 3H). ^{19}F NMR ($CDCl_3$), δ: 62.5. ^{31}P NMR ($CDCl_3$), δ: 2.78, 2.51. ^{13}C NMR ($CDCl_3$), δ: 173.3 (d, J_P = 4.5 Hz), 173.3 (d, J_P = 3.9 Hz), 154.5, 150.3 (d, J_P = 5.3 Hz), 150.3 (d, J_P = 5.1 Hz), 139.5, 135.1, 135.1, 130.9 (q, J_F = 32.2 Hz), 130.8, 129.6, 129.5, 129.1, 129.1, 128.6, 128.6, 128.5, 128.5, 128.2, 128.1, 125.0, 125.0, 124.9, 124.9, 124.4 (q, J_F = 3.8 Hz), 124.3 (q, J_F = 3.9 Hz), 120.0 (d, J_P = 4.7 Hz), 119.9 (d, J_P = 4.8 Hz), 100.4, 99.9, 89.8, 89.8, 84.1 (d, J_P = 7.2 Hz), 84.0 (d, J_P = 7.1 Hz), 75.3, 71.3, 71.2, 67.3, 67.2, 66.2, 66.1, 66.0, 66.0, 50.3 (d, J_P = 1.4 Hz), 50.2 (d, J_P = 0.5 Hz), 20.7, 20.7. UPLC-MS (Method B): t_R 2.22 min, MS [ESI, *m/z*]: 743.1 [M+H$^+$]. HRMS calculated for $C_{34}H_{35}F_3N_6O_8P^+$: 743.2201; found 743.2205.

- Benzyl ((((2R,3S,4R,5R)-3,4-dihydroxy-5-(4-((3-(trifluoromethyl)benzyl)amino)-7*H*-pyrrolo [2,3-d]pyrimidin-7-yl)tetrahydrofuran-2-yl)methoxy)(phenoxy)phosphoryl)-L-alaninate **28**

Obtained as a white sticky solid in 35% yield (diastereomeric mixture with the two diastereomers in a 1:1 ratio). ^{1}H NMR ($CDCl_3$), δ: 8.31–8.23 (m, 2H), 7.65–7.49 (m, 5H), 7.49–7.41 (m, 2H), 7.38–7.27 (m, 11H), 7.22–7.01 (m, 12H), 6.93–6.86 (m, 2H), 6.36–6.29 (m, 2H), 6.05–5.97 (m, 2H, H-1′), 5.21–5.12 (m, 2H), 5.12–5.04 (m, 4H), 4.93–4.86 (m, 4H), 4.34–4.17 (m, 8H), 4.06–3.95 (m, 4H, H-5'), 1.65–1.59 (m, 6H). ^{19}F NMR ($CDCl_3$), δ: 62.4. ^{31}P NMR ($CDCl_3$), δ: 2.66, 2.29. ^{13}C NMR ($CDCl_3$), δ: 175.7 (d, J_P = 4.4 Hz), 175.6 (d, J_P = 3.8 Hz), 172.2, 172.1, 171.5, 171.4, 170.1, 170.0, 134.1, 134.1, 129.8 (m_F), 129.7 (m_F), 128.7, 128.6, 128.2, 128.2, 127.6, 127.6, 127.5, 127.5, 127.4, 127.3, 127.1 (d, J_P = 3,7 Hz), 127.0 (d, J_P = 3,9 Hz), 124.1, 124.1, 123.9, 123.9, 123.4, 123.4, 123.2 (m_F), 123.0 (m_F), 121.4, 121.4, 119.1 (d, J_P = 4.6 Hz), 118.9 (d, J_P = 4.9 Hz), 113.5, 113.5, 89.1, 89.1, 82.5, 82.5, 74.6, 74.6, 70.4, 70.3, 66.5, 66.4, 66.3, 66.3, 65.3 (d, J_P = 5.7 Hz), 65.1 (d, J_P = 4.9 Hz), 49.3, 49.2, 19.8, 19.8. UPLC-MS (Method C): t_R 1.82 min, MS [ESI, *m/z*]: 742.2 [M+H$^+$]. HRMS calculated for $C_{35}H_{36}F_3N_5O_8P^+$: 742.2248; found 742.2253.

4.3. Biological assays

4.3.1. Antiviral and cytotoxicity studies

- Cells and viruses

RD (rhabdomyosarcoma) cells were obtained from the European Collection of Cell Cultures and maintained in minimal essential medium (Gibco) supplemented with 10% heat-inactivated fetal bovine serum (FBS), 1% sodium bicarbonate (Gibco) and 1% L-glutamine (Gibco). Cells were grown at 37 °C and 5% CO_2. The EV71 strain BrCr was kindly provided by F. van Kuppeveld (UMCU, The Netherlands). All other *enteroviruses* belong to the virus collection of the Rega Institute for Medical Research.

The SARS-CoV-2 isolate used was derived from the BetaCov/Belgium/GHB-03021/2020 (EPI ISL407976|2020-02-03), which was isolated from a Belgian patient returning from Wuhan in February 2020, as previously described [48]. The infectious content of the virus stock was determined by titration on Vero E6 cells.

ZIKV (strain MR766, passaged five times in the insect cell line C6/36) was obtained from the European Virus Archive (EVA; http://www.european-virus-archive.com/viruses/zika-virus-strain-mr766), virus stocks were generated and viral titers were determined as previously described [49].

- Antiviral assays

The antiviral assay for EV71 was performed as previously described [16,47,58]. RD cells, grown to confluence in 96-well microtiter plates, were infected with ~100 $CCID_{50}$ of EV71 and treated with a dilution series of the test compounds. Cultures were incubated for three days at 37 °C (5% CO_2), after which residual cell viability was quantified using an MTS readout method according to the manufacturers' instructions (Promega). An analogous assay setup was used for the other *enteroviruses*, with different cell lines (Vero A cells for coxsackievirus B3, and HeLa cells for coxsackievirus A21, enterovirus 68, human rhinovirus A02 and human rhinovirus B14).

The SARS-CoV-2 antiviral assay is based on the previously established SARS-CoV assay [59]. Upon infection the fluorescence of VeroE6-GFP cell cultures declines due to a cytopathogenic effect. In the presence of an antiviral compound, the cytopathogenicity is inhibited and the fluorescent signal maintained. To this end VeroE6-GFP cells (kindly provided by Marnix Van Loock, Janssen Pharmaceutica, Beerse, Belgium), were used as described previously [60]. Since VeroE6 cells show a high efflux of some chemotypes, the antiviral assays were performed in the presence of the P-glycoprotein (Pgp) efflux inhibitor CP-100356 (0.5 μM) [61]. Stock solutions of the test compounds in DMSO (10 mM) were prepared. On day −1, the test compounds were serially diluted in assay medium and the plates were incubated overnight (37 °C, 5% CO_2, and 95% relative humidity). After, Vero E6-eGFP cells were plated corresponding to a final density of 25,000 cells per well in black 96-well plates (Greiner Bio-One, Vilvoorde, Belgium; Catalog 655090). On day 0, cells were infected with SARS-CoV-2 at 20 $CCID_{50}$ per well. Plates were incubated in a humidified incubator at 37 °C and 5% CO_2. At 4 days p.i., wells were examined for eGFP expression using an argon laser-scanning microscope. The microscope settings were excitation at 488 nm and emission at 510 nm, and the fluorescence images of the wells were converted into signal values. Antiviral activity was expressed as EC_{50} defined as the concentration of compound achieving 50% inhibition of the virus-reduced eGFP signals as compared to the untreated virus-infected control cells.

The ZIKV CPE-reduction assay was performed as previously described [49]. Vero E6 cells were grown in growth medium, made of MEM (Life Technologies) supplemented with 10% FCS, 2 mM L-glutamine and 0.075% sodium bicarbonate (Life Technologies). Antiviral assays were performed using the same medium except that 10% FCS was replaced with 2% FCS ('assay medium'). Vero E6 cells were seeded at a density of 104 cells/well in a 96-well plate in 100 μL assay medium and allowed to adhere overnight. To each well 100 μL of culture medium containing 50% cell culture infectious doses ($CCID_{50}$) of ZIKV was added, after which 2-fold serial dilutions of the test compounds were added. Following 5 days of incubation, CPE was determined by means of the MTS readout method and by microscopic evaluation of fixed and

stained cells.

The cytotoxicity of the compounds for Vero E6 cells in the absence of virus was evaluated in a standard MTS assay as previously described [62].

4.3.2. METTL3/METTL14 inhibition assay

The *in-vitro* inhibition assay was performed by Reaction Biology Corp. Malvern, PA, USA, according to the following HotSpot℠ radioisotope reaction system protocol [51].

4.3.2.1. Reaction conditions.

- *METTL3/METTL14 complex* (Active Motif Cat# 31570): Human recombinant full length METTL3 (GenBank Accession No. NP_062826.2) without tag and full length METTL14 (GenBank Accession No. NP_066012.1) with N-terminal FLAG-tag was expressed in Sf9 cells MW = 64.5/53.3 kDa (total 117.8 kDa), 10 nM used in the reaction.

- *METTL3/METTL14 Substrate*: SignalChem cat# M323-58 Oligo ssRNA METTL3/METTL14 Substrate. 5′-rUrArC rArCrU rCrGrA rUrCrU rGrGrA rCrUrA rArArG rCrUrG rCrUrC -3'. 0.75 μM used in the reaction.

- *Methyl donor*: PerkinElmer cat# NET155H001MC. 1 μM S-Adenosyl-L-[methyl-^{3}H]methionine.

- *Reaction buffer*: 50 mM Tris-HCl (pH 8.0), 2 mM MgCl2, 0.01% Brij35, 1 mM DTT, 1% DMSO.

4.3.3. Reagents: all reagents were RNase free

4.3.3.1. Reaction procedure. The substrate (ssRNA) was dissolved in freshly prepared reaction buffer. The enzyme was added into the substrate solution and mixed gently. The compound to test was dissolved in DMSO at different concentrations and added to correspondent enzyme/substrate reaction mixture by using Acoustic Technology (Echo 550, LabCyte Inc. Sunnyvale, CA) in nanoliter range. The mixture was incubated for 20 min at room temperature. 3 H-SAM was added into the reaction mixtures to initiate the reaction. The resulting mixture was incubated for 2 h at room temperature. The reaction mixture was transferred to filter-paper for radioisotopes detection. Data were analyzed using Excel and GraphPad Prism software for IC_{50} curve fits.

Author contributions

Conceptualization, M.B.; methodology, M.B., S.F., M.S., C.V., A.B., J. N. and D.J.; investigation, M.B., M.S., C.V., D.J.; resources, M.B., A.B., S. F., and J.N.; data curation, M.B., M.S. and C.V.; writing—manuscript preparation, M.B., M.S. and C.V.; writing—review and editing, all authors; supervision, M.B., S.F. and D.J.; project administration, M.B.; funding acquisition, M.B. All authors have read and agreed to the published version of the manuscript.

Funding

This research was partly funded by the Sêr Cymru II programme, part-funded by Cardiff and Swansea Universities and the European Regional Development Fund through the Welsh Government.

Declaration of competing interest

The authors declare that they have no known competing financial interests or personal relationships that could have appeared to influence the work reported in this paper.

Data availability

Data will be made available on request.

Appendix A. Supplementary data

Supplementary data to this article can be found online at https://doi.org/10.1016/j.ejmech.2022.114942.

References

[1] H. Zhou, Y. Sun, Y. Guo, Z. Lou, Structural perspective on the formation of ribonucleoprotein complex in negative-sense single-stranded RNA viruses, Trends Microbiol. 21 (2013) 475–484.
[2] P.C. McMinn, An overview of the evolution of enterovirus 71 and its clinical and public health significance, FEMS Microbiol. Rev. 26 (2002) 91–107.
[3] Y. Zhu, Z. Jiang, G. Xiao, S. Cheng, Y. Wen, C. Wan, Circadian rhythm disruption was observed in hand, foot, and mouth disease patients, Medicine (Baltim.) 94 (2015), e601.
[4] A.I. Wells, C.B. Coyne, Enteroviruses: a gut-wrenching game of entry, detection, and evasion, Viruses (2019) 11.
[5] L.Y. Chang, Y.C. Huang, T.Y. Lin, Fulminant neurogenic pulmonary oedema with hand, foot, and mouth disease, Lancet 352 (1998) 367–368.
[6] J. Gu, Y. Zhao, J. Wu, Y. Chen, Y. Yin, X. Jia, L. Mao, Enterovirus-71 utilizes small extracellular vesicles to cross the blood-brain barrier for infecting the central nervous system via transcytosis, J. Med. Virol. (2022), https://doi.org/10.1002/jmv.28120.
[7] J. Hong, F. Liu, H. Qi, W. Tu, M.P. Ward, M. Ren, Z. Zhao, Q. Su, J. Huang, X. Chen, J. Le, X. Ren, Y. Hu, B. Cowling, Z. Li, Z. Chang, Z. Zhang, Changing epidemiology of hand, foot, and mouth disease in China, 2013-2019: a population-based study, Lancet. Reg. Health West Pac. 20 (2022), 100370.
[8] X. Wang, Z. An, D. Huo, L. Jia, J. Li, Y. Yang, Z. Liang, Q. Wang, H. Wang, Enterovirus A71 vaccine effectiveness in preventing enterovirus A71 infection among medically-attended hand, foot, and mouth disease cases, Beijing, China, Hum. Vaccines Immunother. 15 (2019) 1183–1190.
[9] J. Wang, Y. Hu, M. Zheng, Enterovirus A71 antivirals: past, present, and future, Acta Pharm. Sin. B 12 (2022) 1542–1566.
[10] J.Y. Lin, Y.A. Kung, S.R. Shih, Antivirals and vaccines for enterovirus A71, J. Biomed. Sci. 26 (2019) 65.
[11] W. Wen, Z. Qi, J. Wang, The function and mechanism of enterovirus 71 (EV71) 3C protease, Curr. Microbiol. 77 (2020) 1968–1975.
[12] S.K. Swain, A. Gadnayak, J.N. Mohanty, R. Sarangi, J. Das, Does enterovirus 71 urge for effective vaccine control strategies? Challenges and current opinion, Rev. Med. Virol. 32 (2022) e2322.
[13] K.L. Seley-Radtke, M.K. Yates, The evolution of nucleoside analogue antivirals: a review for chemists and non-chemists. Part 1: early structural modifications to the nucleoside scaffold, Antivir. Res. 154 (2018) 66–86.
[14] M.K. Yates, K.L. Seley-Radtke, The evolution of antiviral nucleoside analogues: a review for chemists and non-chemists. Part II: complex modifications to the nucleoside scaffold, Antivir. Res. 162 (2019) 5–21.
[15] M. Arita, T. Wakita, H. Shimizu, Characterization of pharmacologically active compounds that inhibit poliovirus and enterovirus 71 infectivity, J. Gen. Virol. 89 (2008) 2518–2530.
[16] V.E. Oslovsky, M.S. Drenichev, L. Sun, N.N. Kurochkin, V.E. Kunetsky, C. Mirabelli, J. Neyts, P. Leyssen, S.N. Mikhailov, Fluorination of naturally occurring N^6-Benzyladenosine remarkably increased its antiviral activity and selectivity, Molecules 22 (2017).
[17] Z. Yin, Y.-L. Chen, W. Schul, Q.-Y. Wang, F. Gu, J. Duraiswamy, R.R. Kondreddi, P. Niyomrattanakit, S.B. Lakshminarayana, A. Goh, H.Y. Xu, W. Liu, B. Liu, J.Y. H. Lim, C.Y. Ng, M. Qing, C.C. Lim, A. Yip, G. Wang, W.L. Chan, H.P. Tan, K. Lin, B. Zhang, G. Zou, K.A. Bernard, C. Garrett, K. Beltz, M. Dong, M. Weaver, H. He, A. Pichota, V. Dartois, T.H. Keller, P.-Y. Shi, An adenosine nucleoside inhibitor of dengue virus, Proc. Natl. Acad. Sci. USA 106 (2009) 20435–20439.
[18] W. Ye, M. Yao, Y. Dong, C. Ye, D. Wang, H. Liu, H. Ma, H. Zhang, L. Qi, Y. Yang, Y. Wang, L. Zhang, L. Cheng, X. Lv, Z. Xu, Y. Lei, F. Zhang, Remdesivir, (GS-5734) impedes enterovirus replication through viral RNA synthesis inhibition, Front. Microbiol. 11 (2020) 1105.
[19] K.D. Meyer, Y. Saletore, P. Zumbo, O. Elemento, C.E. Mason, S.R. Jaffrey, Comprehensive analysis of mRNA methylation reveals enrichment in 3' UTRs and near stop codons, Cell 149 (2012) 1635–1646.
[20] D. Dominissini, S. Moshitch-Moshkovitz, S. Schwartz, M. Salmon-Divon, L. Ungar, S. Osenberg, K. Cesarkas, J. Jacob-Hirsch, N. Amariglio, M. Kupiec, R. Sorek, G. Rechavi, Topology of the human and mouse m6A RNA methylomes revealed by m6A-seq, Nature 485 (2012) 201–206.
[21] G.D. Williams, N.S. Gokhale, S.M. Horner, Regulation of viral infection by the RNA modification N6-methyladenosine, Annu Rev Virol 6 (2019) 235–253.
[22] H. Hao, S. Hao, H. Chen, Z. Chen, Y. Zhang, J. Wang, H. Wang, B. Zhang, J. Qiu, F. Deng, W. Guan, N6-methyladenosine modification and METTL3 modulate enterovirus 71 replication, Nucleic Acids Res. 47 (2019) 362–374.
[23] M. Yao, Y. Dong, Y. Wang, H. Liu, H. Ma, H. Zhang, L. Zhang, L. Cheng, X. Lv, Z. Xu, F. Zhang, Y. Lei, W. Ye, N(6)-methyladenosine modifications enhance enterovirus 71 ORF translation through METTL3 cytoplasmic distribution, Biochem. Biophys. Res. Commun. 527 (2020) 297–304.

[24] G.-W. Kim, A. Siddiqui, The role of N6-methyladenosine modification in the life cycle and disease pathogenesis of hepatitis B and C viruses, Exp. Mol. Med. 53 (2021) 339–345.
[25] Z. Feng, F. Zhou, M. Tan, T. Wang, Y. Chen, W. Xu, B. Li, X. Wang, X. Deng, M. L. He, Targeting m6A modification inhibits herpes virus 1 infection, Genes Dis 9 (2022) 1114–1128.
[26] N. Li, H. Hui, B. Bray, G.M. Gonzalez, M. Zeller, K.G. Anderson, R. Knight, D. Smith, Y. Wang, A.F. Carlin, T.M. Rana, METTL3 regulates viral m6A RNA modification and host cell innate immune responses during SARS-CoV-2 infection, Cell Rep. 35 (2021), 109091.
[27] X. Wang, B.S. Zhao, I.A. Roundtree, Z. Lu, D. Han, H. Ma, X. Weng, K. Chen, H. Shi, C. He, N(6)-methyladenosine modulates messenger RNA translation efficiency, Cell 161 (2015) 1388–1399.
[28] X. Wang, Z. Lu, A. Gomez, G.C. Hon, Y. Yue, D. Han, Y. Fu, M. Parisien, Q. Dai, G. Jia, B. Ren, T. Pan, C. He, N6-methyladenosine-dependent regulation of messenger RNA stability, Nature 505 (2014) 117–120.
[29] C. Zeng, W. Huang, Y. Li, H. Weng, Roles of METTL3 in cancer: mechanisms and therapeutic targeting, J. Hematol. Oncol. 13 (2020) 117.
[30] R.K. Bedi, D. Huang, S.A. Eberle, L. Wiedmer, P. Śledź, A. Caflisch, Small-molecule inhibitors of METTL3, the major human epitranscriptomic writer, ChemMedChem 15 (2020) 744–748.
[31] E. Yankova, W. Blackaby, M. Albertella, J. Rak, E. De Braekeleer, G. Tsagkogeorga, E.S. Pilka, D. Aspris, D. Leggate, A.G. Hendrick, N.A. Webster, B. Andrews, R. Fosbeary, P. Guest, N. Irigoyen, M. Eleftheriou, M. Gozdecka, J.M.L. Dias, A. J. Bannister, B. Vick, I. Jeremias, G.S. Vassiliou, O. Rausch, K. Tzelepis, T. Kouzarides, Small-molecule inhibition of METTL3 as a strategy against myeloid leukaemia, Nature 593 (2021) 597–601.
[32] N. Kumar, S. Sharma, R. Kumar, B.N. Tripathi, S. Barua, H. Ly, B.T. Rouse, Host-directed antiviral therapy, Clin. Microbiol. Rev. 33 (2020) e00168-00119.
[33] H. Song, J. Song, M. Cheng, M. Zheng, T. Wang, S. Tian, R.A. Flavell, S. Zhu, H. B. Li, C. Ding, H. Wei, R. Sun, H. Peng, Z. Tian, METTL3-mediated m(6)A RNA methylation promotes the anti-tumour immunity of natural killer cells, Nat. Commun. 12 (2021) 5522.
[34] S. Locarnini, S. Bowden, Drug resistance in antiviral therapy, Clin. Liver Dis. 14 (2010) 439–459.
[35] Y.K. Gupta, S.H. Chan, S.Y. Xu, A.K. Aggarwal, Structural basis of asymmetric DNA methylation and ATP-triggered long-range diffusion by EcoP15I, Nat. Commun. 6 (2015) 7363.
[36] X. Wang, J. Feng, Y. Xue, Z. Guan, D. Zhang, Z. Liu, Z. Gong, Q. Wang, J. Huang, C. Tang, T. Zou, P. Yin, Structural basis of N6-adenosine methylation by the METTL3–METTL14 complex, Nature 534 (2016) 575–578.
[37] K. Goedecke, M. Pignot, R.S. Goody, A.J. Scheidig, E. Weinhold, Structure of the N6-adenine DNA methyltransferase M.TaqI in complex with DNA and a cofactor analog, Nat. Struct. Biol. 8 (2001) 121–125.
[38] S.P. Lim, L.S. Sonntag, C. Noble, S.H. Nilar, R.H. Ng, G. Zou, P. Monaghan, K. Y. Chung, H. Dong, B. Liu, C. Bodenreider, G. Lee, M. Ding, W.L. Chan, G. Wang, Y. L. Jian, A.T. Chao, J. Lescar, Z. Yin, T.R. Vedananda, T.H. Keller, P.Y. Shi, Small molecule inhibitors that selectively block dengue virus methyltransferase, J. Biol. Chem. 286 (2011) 6233–6240.
[39] D. Cheng, V. Vemulapalli, M.T. Bedford, Methods applied to the study of protein arginine methylation, Methods Enzymol. 512 (2012) 71–92.
[40] P. Serafinowski, E. Dorland, K.R. Harrap, J. Balzarini, E. De Clercq, Synthesis and antiviral activity of some new S-adenosyl-L-homocysteine derivatives, J. Med. Chem. 35 (1992) 4576–4583.
[41] Schrödinger Release 2020-2: Glide, Schrödinger, LLC, New York, NY, 2020.
[42] J. Li, H. Wei, M.-M. Zhou, Structure-guided design of a methyl donor cofactor that controls a viral histone H3 lysine 27 methyltransferase activity, J. Med. Chem. 54 (2011) 7734–7738.
[43] R. Srivastava, A. Bhargava, R.K. Singh, Synthesis and antimicrobial activity of some novel nucleoside analogues of adenosine and 1,3-dideazaadenosine, Bioorg. Med. Chem. Lett 17 (2007) 6239–6244.
[44] D.E. McCloskey, S. Bale, J.A. Secrist III, A. Tiwari, T.H. Moss III, J. Valiyaveettil, W. H. Brooks, W.C. Guida, A.E. Pegg, S.E. Ealick, New insights into the design of inhibitors of human S-adenosylmethionine decarboxylase: studies of adenine C8 substitution in structural analogues of S-adenosylmethionine, J. Med. Chem. 52 (2009) 1388–1407.
[45] H. Vorbrüggen, B. Bennua, Nucleoside syntheses, XXV1) A new simplified nucleoside synthesis, Chem. Ber. 114 (1981) 1279–1286.
[46] R. Rayala, P. Theard, H. Ortiz, S. Yao, J.D. Young, J. Balzarini, M.J. Robins, S. F. Wnuk, Synthesis of purine and 7-deazapurine nucleoside analogues of 6-N-(4-Nitrobenzyl)adenosine; inhibition of nucleoside transport and proliferation of cancer cells, ChemMedChem 9 (2014) 2186–2192.
[47] K. Lanko, C. Shi, S. Patil, L. Delang, J. Matthijnssens, C. Mirabelli, J. Neyts, Assessing in vitro resistance development in enterovirus A71 in the context of combination antiviral treatment, ACS Infect. Dis. 7 (2021) 2801–2806.
[48] D. Bardiot, L. Vangeel, M. Koukni, P. Arzel, M. Zwaagstra, H. Lyoo, P. Wanningen, S. Ahmad, L. Zhang, X. Sun, A. Delpal, C. Eydoux, J.C. Guillemot, E. Lescrinier, H. Klaassen, P. Leyssen, D. Jochmans, K. Castermans, R. Hilgenfeld, C. Robinson, E. Decroly, B. Canard, E.J. Snijder, M.J. van Hemert, F. van Kuppeveld, P. Chaltin, J. Neyts, S. De Jonghe, A. Synthesis Marchand, Structure-activity relationships, and antiviral profiling of 1-heteroaryl-2-alkoxyphenyl analogs as inhibitors of SARS-CoV-2 replication, Molecules 27 (2022).
[49] J. Zmurko, R.E. Marques, D. Schols, E. Verbeken, S.J. Kaptein, J. Neyts, The viral polymerase inhibitor 7-deaza-2'-C-methyladenosine is a potent inhibitor of in vitro Zika virus replication and delays disease progression in a robust mouse infection model, PLoS Neglected Trop. Dis. 10 (2016), e0004695.
[50] L. Vangeel, W. Chiu, S. De Jonghe, P. Maes, B. Slechten, J. Raymenants, E. André, P. Leyssen, J. Neyts, D. Remdesivir Jochmans, Molnupiravir and Nirmatrelvir remain active against SARS-CoV-2 Omicron and other variants of concern, Antivir. Res. 198 (2022), 105252.
[51] K.Y. Horiuchi, M.M. Eason, J.J. Ferry, J.L. Planck, C.P. Walsh, R.F. Smith, K. T. Howitz, H. Ma, Assay development for histone methyltransferases, Assay Drug Dev. Technol. 11 (2013) 227–236.
[52] M.A. Caudill, J.C. Wang, S. Melnyk, I.P. Pogribny, S. Jernigan, M.D. Collins, J. Santos-Guzman, M.E. Swendseid, E.A. Cogger, S.J. James, Intracellular S-adenosylhomocysteine concentrations predict global DNA hypomethylation in tissues of methyl-deficient cystathionine β-synthase heterozygous mice, J. Nutr. 131 (2001) 2811–2818.
[53] Y. Mehellou, H.S. Rattan, J. Balzarini, The ProTide prodrug Technology: from the concept to the clinic, J. Med. Chem. 61 (2018) 2211–2226.
[54] M. Serpi, K. Madela, F. Pertusati, M. Slusarczyk, Synthesis of phosphoramidate prodrugs: ProTide approach, Curr Protoc Nucleic Acid Chem (2013) (Chapter 15), Unit15.15.
[55] version Flare, Litlington Cresset®, U.K. Cambridgeshire. http://www.cresset-group.com/flare/.
[56] T. Cheeseright, M. Mackey, S. Rose, A. Vinter, Molecular field extrema as descriptors of biological activity: definition and validation, J. Chem. Inf. Model. 46 (2006) 665–676.
[57] 50. Molecular Operating Environment (MOE 2019.10); Chemical Computing Group, Inc.: Montreal, QC, Canada. Available online: http://www.chemcomp.com (accessed on 29 July 2022).
[58] A. Tijsma, D. Franco, S. Tucker, R. Hilgenfeld, M. Froeyen, P. Leyssen, J. Neyts, The capsid binder Vapendavir and the novel protease inhibitor SG85 inhibit enterovirus 71 replication, Antimicrob. Agents Chemother. 58 (2014) 6990–6992.
[59] T. Ivens, C. Van den Eynde, K. Van Acker, E. Nijs, G. Dams, E. Bettens, A. Ohagen, R. Pauwels, K. Hertogs, Development of a homogeneous screening assay for automated detection of antiviral agents active against severe acute respiratory syndrome-associated coronavirus, J. Virol. Methods 129 (2005) 56–63.
[60] T.N.D. Do, K. Donckers, L. Vangeel, A.K. Chatterjee, P.A. Gallay, M.D. Bobardt, J. P. Bilello, T. Cihlar, S. De Jonghe, J. Neyts, D. Jochmans, A robust SARS-CoV-2 replication model in primary human epithelial cells at the air liquid interface to assess antiviral agents, Antivir. Res. 192 (2021), 105122.
[61] R.L. Hoffman, R.S. Kania, M.A. Brothers, J.F. Davies, R.A. Ferre, K.S. Gajiwala, M. He, R.J. Hogan, K. Kozminski, L.Y. Li, J.W. Lockner, J. Lou, M.T. Marra, L. J. Mitchell Jr., B.W. Murray, J.A. Nieman, S. Noell, S.P. Planken, T. Rowe, K. Ryan, G.J. Smith III, J.E. Solowiej, C.M. Steppan, B. Taggart, Discovery of ketone-based covalent inhibitors of coronavirus 3CL proteases for the potential therapeutic treatment of COVID-19, J. Med. Chem. 63 (2020) 12725–12747.
[62] D. Jochmans, P. Leyssen, J. Neyts, A novel method for high-throughput screening to quantify antiviral activity against viruses that induce limited CPE, J. Virol. Methods 183 (2012) 176–179.